Compton scattering on the proton at low and medium energies

P. S. Baranov and L. V. Fil'kov

P. N. Lebedev Physics Institute, Academy of Sciences of the USSR, Moscow

Fiz. Elem. Chastits At. Yadra. 7, 108–185 (January–March 1976)

The experimental and theoretical investigations into the elastic scattering of γ rays on protons at low and medium energies are reviewed. Dispersion relations and dispersion sum rules for the γN scattering amplitudes are constructed and analyzed. The sign of the $\pi^0 \to 2\gamma$ decay amplitude is found. The experimental γp scattering cross sections at γ energies $\nu \lesssim 100$ MeV are used to determine the coefficients of the electric and magnetic polarizability of the proton.

PACS numbers: 13.60.Dx, 11.50.Li, 13.20.Cz

INTRODUCTION

Compton scattering on the proton at low and intermediate energies is considered in this review. Compton scattering on a nucleon yields valuable information about the electromagnetic and strong interactions of the particles involved.

At low energies (up to 100 MeV) the cross section for the scattering of γ rays on a nucleon can be represented as a series expansion in the energy of the γ. When the expressions for the cross sections are compared with the experimental data, one can obtain important characteristics like the electric and magnetic polarizabilities of the proton.

If the incident γ has energy greater than 100 MeV, strong interactions in intermediate states acquire decisive importance. Then the only consistent method of analysis for the process is by dispersion relations. In this case, we have integral relations between the γN scattering amplitudes and quadratic functions of the photoproduction and $NN \to \gamma\gamma$ annihilation amplitudes. Therefore, from comparison with experimental data one can determine the unknown parameters introduced into the theory; for example, one can determine the sign of the $\pi^0 \to 2\gamma$ decay amplitude, which is an important parameter in different models of elementary-particle interaction. It follows from what we have said that one of the most interesting fields of investigation in γp scattering is that with incident γ's having energies $\nu \lesssim 350$ MeV. This restriction is necessary because the information about the photoproduction of two or more pions or the photoproduction of heavier particles needed for the theoretical calculations is sparse, and these reactions can make an important contribution to the γp scattering cross section above 350 MeV. Thus, additional unknown parameters must be introduced into the theory if dispersion relations are to be used in this energy range.

For this reason, only phenomenological methods based on resonance models are used in the energy range 400 MeV $\lesssim \nu < 1$ GeV. Study of γp scattering at these energies is of interest from the point of view of the phenomenological investigation of resonances. Thus, γp scattering is more suitable than photoproduction for determining the radiative decay widths of resonances, which enter in this case quadratically.

In this review, we consider in detail γp scattering only at low and medium energies up to $\nu \lesssim 350$ MeV, where the theoretical predictions are best confirmed and the most important results have been obtained.

1. EXPERIMENTAL INVESTIGATION OF THE ELASTIC SCATTERING OF GAMMA RAYS ON PROTONS

Methods of identifying elastic scattering of gamma rays on protons

One might think it would be easy to identify the reaction

$$\gamma + p \to \gamma' + p' \tag{1}$$

by observing both particles in the final state. In reality, the experimental investigation of the elastic scattering of γ rays on protons entails considerable experimental difficulties, which are due to the very small cross section ($\sim 10^{-32}$ cm^2/sr) and the presence of strong background processes. In the investigation of the elastic scattering of γ rays on protons at low energies up to about 100 MeV there are additional difficulties associated with the low energies of the recoil protons.

In this energy range of the γ's, it is virtually impossible to separate the elastic scattering reaction by the simultaneous detection of the two particles—the recoil proton and the scattered γ—and the process (1) is studied by detecting only the scattered γ in angular and energy regions that are free of γ's produced by the background processes.

The main background process at energies below the threshold of single pion photoproduction is the radiative formation of electron-positron pairs: the process of pair creation in the field of the nucleus with subsequent emission of a γ through bremsstrahlung by one of the electrons in the same field.

In Refs. 1 and 2, the cross sections of this background process were calculated and they indicated significant corrections for small scattering angles. Experiments made at MIT (see Ref. 3) showed that the radiative pair creation has a pronounced peaking with respect to the spatial direction and a strong energy dependence. The contribution of this process for the angle 70° is 10%, while at 45° it appreciably exceeds the yield of γ's from the elastic scattering.

Other background processes also have a pronounced angular peaking; these include single processes such as Compton scattering of γ's on electrons, pair creation, splitting of a photon into two photons in the Coulomb field of the nucleus,[4,5] as well as multiple background processes such as pair creation at large angles[6] with subsequent bremsstrahlung in the target or parts of the instrument.

The difficulties of making exact calculations for some

TABLE I.

Result			Laboratory, country	Experimental paper
Energy in lab. system, MeV	Angle in lab. system, deg	Cross section in lab. system, 10^{-32} cm²/sr		
1.6	124±3	1.46±0.25	California Institute of Technology, USA	[8]
40—70 (55)	45	3.40±0.28	P.N. Lebedev Physics Institute, USSR	[9]
	75	1.12±0.08		
	90	1.10±0.05		
	120	1.34±0.08		
	135	1.56±0.08		
	150	1.93±0.07		
30—95	50	4.8±0.4 → 3.1	University of Chicago, USA	[10] *
	60	2.8±0.15 → 2.3		
	70	1.5±0.12 → 1.3		
	90	1.05±0.11		
	120	1.25±0.11		
	150	1.39±0.11		
30—90 (60)	60	1.80±0.14	University of Chicago, USA	[11]
	90	1.03±0.08		
	120	1.25±0.10		
	150	1.39±0.11		
25—87	70	1.06±0.08	University of Chicago, USA	[12]
	90	1.08±0.04		
	120	1.18±0.05		
	150	1.47±0.06		
75—119 (97)	45	1.40±0.17	P.N. Lebedev Physics Institute, USSR	[13]
	90	1.35±0.13		
	135	2.25±0.45		
70^{+24}_{-26}	90±16	1.26±0.08	University of California, USA	[14]
$100^{+9.5}_{-7.5}$	90±16	1.50±0.40		
123^{+10}_{-8}	90±16	1.83±0.52		
104.4	76.0±3.6	1.41±0.11	P.N. Lebedev Physics Institute, USSR	[15, 16]
80.9	90.0±3.6	1.15±0.06		
85.4	90.0±3.6	1.09±0.04		
109.9	90.0±3.6	1.03±0.06		
81.9	150.0±3.5	1.44±0.12		
86.3	150.0±3.5	1.37±0.10		
106.7	150.0±3.5	1.60±0.08		
111.1	150.0±3.5	1.44±0.06		
54.0	90	1.09±0.17	MIT, USA	[3]
64.8	90	1.09±0.21		
75.0	90	1.09±0.16		
84.5	90	1.08±0.17		
90.5	90	1.07±0.17		
102	90	1.05±0.12		
113	90	1.04±0.15		
125	90	0.98±0.28		
135	90	0.93±0.52		

*The data of this paper are taken from the figures.

of the background processes prevents one from taking into account accurately their contributions to the experimentally measured yield. Thus, neither experimentally or computationally can one obtain sufficiently accurate estimates of the background for scattering angles less than 45°. This explains the complete absence of experimental data on the elastic scattering of γ's on protons in this range of angles.

The range of γ energies directly above the threshold of single pion photoproduction is especially difficult for experimental investigation. Elastic scattering on protons in this energy range cannot be identified by observation of the scattered γ ray alone since the energy resolution of the γ detectors is inadequate to distinguish by means of the energy the γ's from the elastic scattering (1) and from decay of neutral pions into γ's in the photoproduction process

$$\gamma + p \to p + \pi^0, \quad \pi^0 \to \gamma + \gamma \qquad (2)$$

At γ energies around 200 MeV, the cross section of the photoproduction reaction (2) is almost two orders of magnitude greater than the cross section of elastic scattering of γ's on protons, and the final products of the reaction (2) are the same particles as in the reaction (1) but with slightly lower energies. The energy of the protons can be determined sufficiently accurately to distinguish these reactions by the energies of the recoil protons, and this makes it necessary to observe the protons as well. However, because of the continuous spectrum of primary γ's from the accelerator, to separate out the elastic scattering process it is necessary to define the energy interval of the primary γ's clearly; usually, this is done by discrimination with respect to the energy of the detected protons. As a rule, the energy range of the primary γ's is situated near the upper limit of the bremsstrahlung spectrum. This leads, on the one hand, to an appreciable lowering of the reaction yield due to the fewer γ's in the selected energy range and, on the other, imposes stringent requirements on the stability of the maximal energy in the bremsstrahlung spectrum and on the accuracy of its determination.

The yield from the elastic scattering of γ's on protons above the pion photoproduction threshold is lower than below the threshold, when the process can be identified by the γ alone, because the recoil protons in this energy range still have short ranges, which prevents one from making full use of liquid-hydrogen targets a few centimeters thick.

It should be pointed out that the detection of only the protons in a small energy range near the end of the bremsstrahlung spectrum does not yet enable one to distinguish the elastic scattering process.

An appreciable background of protons (two orders greater than the effect) comes from the thin walls of the target containing the liquid hydrogen. An effective way of eliminating this background is to detect both products of the reaction (1), i. e., the recoil proton and the scattered γ. The difficulties discussed here mean that the range 150—200 MeV of γ energies has hitherto hardly been investigated.

At higher γ energies, the difference between the energies of the recoil protons from elastic scattering and from pion photoproduction on hydrogen is less, which leads to additional difficulties in identification of the elastic scattering of the γ's also in the region of higher energies. These difficulties were overcome in Ref. 7 by the use of spark chambers to detect not only the protons but also the γ's, which made it possible to determine the spatial coordinates of the particles and separate out kinematically the elastic scattering process on the smoothly varying background of the pion photoproduction.

Experimental data on the elastic scattering of gamma rays on protons

The experimental investigation of the elastic scattering of γ's on protons was begun in the middle of the fifties. These investigations were first concentrated on the region of low γ energies, corresponding to the energies achieved at that time in electron accelerators. Then, as accelerator technology developed, the range of the investigations was gradually extended to higher energies and, in the last few years, has been pushed up to 18 GeV. Tables 1 and 2 give the experimental data in the energy range up to about 2 GeV: in Table 1 at low energies in the laboratory system, and in Table 2 all the existing experimental data in the center of mass system. In setting up Table 2, we converted the experimental data published originally for the laboratory system to the center-of-mass system. Tables 1 and 2 also

TABLE II.

Result			Laboratory, country	Experimental paper
Energy in the lab.system, MeV	Cms angle, deg	Cms cross section, 10^{-32} cm^2/sr		
1.6	124	1.45±0.25	California Institute of Technology, USA	[8]
30—95 (60)	52.7	4.45±0.4→2.9	University of Chicago, USA	[10]
	63.0	2.64±0.14→2.2		
	73.3	1.44±0.12		
	93.3	1.05±0.11		
	122.4	1.33±0.11		
	151.7	1.45±0.12		
	63.0	1.70±0.13	The same	[11] *
30—90 (60)	93.5	1.07±0.08		
	122.7	1.33±0.11		
	151.7	1.54±0.12		
25—87	73.3	1.02±0.08	» »	[12]
	93.5	1.08±0.04		
	122.7	1.26±0.05		
	151.7	1.63±0.07		
75—119 (97)	48.8	1.24±0.15	P.N. Lebedev Physics Institute, USSR	[13]
	95.2	1.36±0.13		
	138.7	2.57±0.51		
	47.2	3.15±0.26	The same	[9]
40—70 (55)	78.1	1.09±0.08		
	93.2	1.10±0.05		
	122.7	1.42±0.08		
	137.2	1.69±0.09		
	151.5	2.13±0.08		
104.4	80.0	1.31±0.10	» »	[16, 15]
80.9	94.6	1.16±0.06		
85.4	94.7	1.10±0.04		
109.9	95.6	1.03±0.06		
81.9	152.1	1.62±0.13		
86.3	152.2	1.56±0.11		
106.7	152.6	1.88±0.08		
111.1	152.7	1.70±0.07		
70	94.3	1.57±0.09	University of California, USA	[14]
100	95.6	1.88±0.50		
123	96.7	2.29±0 65	MIT, USA	[3]*
54.0	93.08	1.08±0.17		
64.8	93.75	1.08±0.21		
75.0	94.33	1.09±0.16		
84.5	94.75	1.09±0.17		
90.5	95.08	1.08±0.17		
101.7	95.67	1.04±0.11		
113.0	96.17	1.08±0.14		
125.0	96.58	0.98±0.30		
135.0	96.83	0.94±0.50	P.N. Lebedev Physics Institute, USSR	[17]
182.0	94.8	2.00±0.28		
195.0	94.6	1.49±0.24		
210.0	93.5	1.91±0.56		
235.0±12.7	55.4±1.4	4.24±0.57	P.N. Lebedev Physics Institute, USSR	[18, 19]
239.5±9.8	69.5±1.3	6.08±0.76		
247.4±5.3	92.6±1.1	6.06±0.70		
248.0±4.9	108.4±1.1	9.56±1.02		
248.3±4.3	131.8±1.2	9.13±0.78		
248.1±4.4	147.5±1.1	12.79±1.07		
247.8±7.5	70.0±1.2	7.13±0.85	The same	[20]
248.1±5.9	93.0±1.2	6.66±0.55		
248.8±5.3	108.4±1.2	8.54±0.65		
248.5±4.5	131.9±1.5	9.59±0.63		
249.2±4.2	147.7±1.3	13.02±0.70		
215.4±8.4	68.8±1.3	3.28±0.34		
214.7±6.7	91.9±1.4	1.86±0.20		
215.2±7.4	107.2±1.3	2.49±0.26		
212.9±6.5	131.4±1.6	4.25±0.35		
213.4±5.5	147.4±1.3	6.58±0.41		
206—248 (230)	65.1—72.9 (70)	5.34±0.4	University of Illinois, USA	[21]
178—206 (193)	86.1—98.1 (90)	1.92±0.23		
290—225 (213)	88.0—96.0 (90)	3.38±0.71		
228—248 (239)	87.7—95.8 (90)	6.80±0.71		
232—248 (240)	85.7—97.8 (90)	8.25±0.94		
252—272 (262)	87.6—95.6 (90)	13.38±1.41		
257—272 (267)	87.6—95.6 (90)	17.28±4.23		
265—283 (276)	87.5—95.5 (90)	13.11±1.65		
271—288 (282)	87.4—95.4 (90)	18.04±4.7		
186—206 (197)	125.5—133.5 (129)	3.64±0.94		
230—248 (239)	125.0—133.1 (129)	12.37±1.18		
112—127 (120)	136—144 (139)	1.76±0.23		
132—144 (139)	135.8—144 (139)	2.28±0.23		
156—170 (163)	135.7—143.7 (139)	2.16±0.23		
176—193 (184)	135.6—143.6 (139)	2.98±0.28		
192—208 (200)	135.5—143.5 (139)	5.30±0.71		
220—233 (227)	135.3—143.3 (139)	7.67±0.94		

Continuation of Table 2

Result			Laboratory, country	Experimental paper
Energy in the lab. system, MeV	Cms angle, deg	Cms cross section 10^{-32} cm^2/sr		
266—285 (275.5)	92	15.5±3.1	University of Illinois, USA	[22]
285—335 (310)	90	14.5±1.6		
185—235 (210)	142	4.42±0.76		
235—285 (260)	138	15.2±1.6		
285—335 (310)	136	21.3±1.8		
Experiments made with polarized beam of γ's. Measurement made of ratio of cross sections in the plane of the polarization and perpendicular to it:			Frascati, Italy	[23]
305—335	90	$2.1^{+0.5}_{-0.4}$		
Measurement made of the degree of polarization of the recoil protons.			Tokyo University, Japan	[24]
700	90	0.39±0.26		
800	90	0.23±0.26		
236.9	90.0	4.6±0.5	Physics Institute of the Bonn University, West Germany	[25, 26]
238.6	110.0	4.7±0.8		
249.1	130.0	5.8±1.0		
265.6	69.9	6.3±0.9		
272.6	90.0	9.8±0.8		
279.7	109.9	9.7±0.7		
284.6	70.1	12.9±1.0		
285.0	129.9	13.5±1.1		
289.4	90.2	11.6±0.8		
316.9	70.2	19.5±1.3		
323.1	60.0	21.8±1.5		
329.4	90.0	13.2±0.9		
329.4	110.1	15.5±0.9		
334.8	130.0	16.4±1.1		
367.4	49.8	14.9±1.5		
370.8	69.8	13.8±1.0		
380.6	89.7	9.9±0.6		
382.4	109.7	8.6±0.7		
386.5	129.6	10.5±0.8		
406.7	50.0	10.2±1.3		
407.8	89.9	8.6±1.9		
415.8	69.9	7.5±0.8		
420.8	89.8	7.7±0.6		
427.4	109.9	6.7±0.4		
429.4	130.0	7.4±0.7		
725—775	60	3±3	Cornell University, USA	[27]
300—325	75	18.0±1.6		
300—350	75	19.5±2.6		
275—300	90	15.8±1.1		
300—325	90	14.3±0.9		
350—375	90	13.3±1.3		
400—425	90	12.0±1.7		
300—315	120	20.6±2.1		
250	90±10	4.2±1.0	Physics Institute of the Bonn University, West Germany	[28] *
300	90±10	12.2±1.4		
350	90±10	15.1±1.0		
400	90±10	9.2±1.5		
380±10	50	14.0±1.2		
	70	12.3±0.8		
	90	8.8±0.6		
	110	7.3±0.6		
	130	8.4±0.7		
400—430	50	8.5±1.0	The same	[25]
	70	7.0±0.7		
	90	6.7±0.5		
	110	5.4±0.4		
	130	5.7±0.5		
314±14	90.3±4.4	12.4±3.0	Tokyo University, Japan	[29]
351±22	90.0±4.6	15.2±2.2		
416±11	89.4±4.6	11.1±2.5		
437±10	89.2±4.6	9.6±3.2		
456±12	88.9±4.7	5.1±1.9		
512±15	88.4±4.7	6.2±2.8		
541±14	88.1±4.8	8.7±3.1		
616±24	87.3±4.8	7.4 ±2.4		
692±25	86.5±4.8	6.0±1.6		
535	90	6.37±0 63	MIT, USA	[7]
570	90	6.94±0.63		
602	90	8.20±0.63		
633	90	9.30±0.70		
665	90	8.96±0.70		
695	90	11.0±0.82		
726	90	10.25±0.82		
755	90	9.68±0.89		
783	90	8.96±0.89		
812	90	9.24±0.89		
842	90	7.26±0.70		
480	90	10.0±0.8	Cornell University, USA	[30] *
520	90	8.1±0.6		
565	90	7.6±0.6		
610	90	8.2±0.8		
660	90	7.9±0.8		
660	90	9.0±1.0		
705	90	8.7±1.0		
715	90	8.4±1.0		
740	90	8.5±1.2		
770	90	8.7±1.1		
785	90	8.6±1.0		
820	90	7.0±0.9		

Continuation of Table 2

Result			Laboratory, country	Experimental paper
Energy in the lab. system, MeV	Cms angle, deg	Cms cross section 10^{-32} cm²/sr		
830	90	7.4±0.8	Cornell University, USA	[30] *
865	90	6.4±0.9		
890	90	6.9±0.9		
900	90	6.2±0.8		
945	90	5.3±0.8		
955	90	6.0±0.9		
985	90	6.0±1.0		
1025	90	5.5±0.9		
1065	90	6.5±1.0		
1100	90	5.1±1.0		
1160	90	2.7±0.6		
1185	90	1.6±0.8		
1250	90	1.8±0.8		
1270	90	2.3±0.9		
1360	90	3.9±1.8		
1420	90	4.2±2.3		
568		5.2	The same	[31]
598		4.1		
630		7.2		
658		9.15		
688		9.1		
719		9.5		
720		9.0		
750		12.5		
770		10.0		
780		12.4		
800		9.0		
810		11.0		
840		10.3		
855		9.0		
910		8.2		
955		7.5		
1010		6.2		
1060		4.8		
1120		5.1		
1165		3.8		
1220		3.5		
1250		2.1		
870		11.3	MIT, USA	According to the the authors, the statistical errors are 10–15%.
920		7.7		
970		6.0		
1040		4.7		
1070		3.4		
1115		4.8		
1150		4.2		
1178		3.8		
1208		3.1		
1223		2.5		
1263		3.0		
1300	65	2.4		
1300	65	2.1		
1370	65	1.6		
1445	65	1.8		
1530	65	1.5		
1580	65	1.2		
1680	65	1.2		
1735	65	1.1		
1825	65	0.8		
1890	65	1.5		

*The data of this paper are taken from the figures.

include the experimental data that were published in figures in the original papers. The error involved in taking the cross sections from the graphs of the original publications is 0.2×10^{-32} cm² sr, and for the energies it is 2–3%.

The complete experimental data obtained so far on the Compton effect on the proton can be divided into three groups: energies up to 120 MeV, energies from the threshold of single pion photoproduction up to about 400 MeV, and the range of higher energies. This is a convenient subdivision: First, different experimental methods are used to identify the elastic scattering process in these different ranges of γ energies, and, second, the theoretical relevance of the investigations is different in the different regions.

Let us consider in more detail the experiments made at low and medium energies.

Description of experiments on the elastic scattering of gamma rays on protons

Experiments up to 120 MeV. The elastic scattering of γ rays on protons in the energy range from 1 to 120 MeV has been carried out basically in four laboratories: the P. N. Lebedev Physics Institute of the Academy of Sciences of the USSR,[9,13,15,16,32] the University of Chicago in the USA,[10–12] MIT in the USA,[33] and the University of California in the USA.[14] The main characteristics of the experimental apparatus used in these investigations are given in Table 3.

It can be seen from Table 3 that all experimental investigations in this energy range were made on cyclic electron accelerators operating under conditions with maximal electron energy and, therefore, with maximal energy of the bremsstrahlung spectrum of the γ's that did not exceed the threshold of single pion photoproduction. Some of these accelerators have now been dismantled or reconstructed for use at higher energies (in Table 3 these are indicated by an asterisk). In all the low-energy investigations a similar method was used; it is based on detection of the scattered γ's by means of scintillation counter telescopes connected in coincidence. The principle of operation of these telescopes consists of the detection of the electrons of a pair that are produced by conversion of the γ's in a lead converter placed in front of the coincidence counters. To avoid the detection of charged particles, above all electrons, one further scintillation counter connected in anticoincidence is placed in front of the converter. The efficiency of this counter was usually about 98%. However, if one takes into account the high background and the small cross section of the effect to be measured, this means alone is inadequate, and therefore, to reduce the loading of the telescope counters with slow electrons and soft γ's, additional absorbers of a light material (beryllium, paraffin, carbon), whose thicknesses are given in Table 3, were usually placed in front of the telescope.

The efficiency of detecting γ's by the counter telescope was usually measured experimentally, in different ways, and was about 30%. It should be said that the least successful methods of determining the efficiency were those used in Refs. 3 and 14, in which the telescopes were placed directly in the bremsstrahlung beam with intensity reduced by a factor 10^5–10^6; in this case it was not possible to guarantee the required high accuracy of measurement of the reduced intensity. The energy range of the γ's in the telescopes was fixed as follows. The lower end of the detection interval was determined by the thicknesses of the scintillation counters and the intermediate absorbers between the counters. The upper end was determined by the maximal energy of the bremsstrahlung spectrum.

The conditions of operation with γ energies near the upper end of the bremsstrahlung spectrum have two shortcomings: 1) The number of γ's in the bremsstrahlung spectrum decreases rapidly with increasing energy, which seriously reduces the observed reaction yield, and there is a high background of electrons and low-energy γ's; 2) instability of the maximal energy of 1–2% changes the detection interval by 5–10%, and therefore leads to a large additional uncertainty in the measured differential cross section. Therefore, to detect

TABLE III.

Experimental paper	[10]	[11]	[12]	[13]	[9]	[32]	[33]	[3,23]	[14]
Characteristics and accelerator type	Betatron, University of Chicago, USA			265-MeV	P.N. Lebedev Physics Institute Synchrotron		Synchrotron*, MIT, USA		330-MeV Synchrotron*, University of California, USA
Maximal energy, MeV	98	98	87	120	75	127–148	140	140	95–113–132
Monitoring of γ beam	Reaction $^{12}C(\gamma,n)^{11}C$	Reaction $^{12}C(\gamma,n)^{11}C$	Thick-wall ionization chamber. Reaction $^{12}C(\gamma,n)^{11}C$	–	Thick-wall ionization chamber. Reaction $^{12}C(\gamma,n)^{11}C$	Quantameter. Reaction $^{12}C(\gamma,n)^{11}C$	Thick-wall ionization chamber	–	Thick-wall ionization chamber
Detector of γ's: type	Scintillation counter telescope, ACC	Scintillation counter telescope, ACC	Scintillation counter telescope, ACC	Scintillation counter telescope, ACCC	Scintillation counter telescope, ACCC	Scintillation counter telescope, ACCCCA	Scintillation counter telescope. Last counter total absorption type. $ACCC_a$	Scintillation counter telescope. Last counter total absorption type. $ACCC_a$	Scintillation counter telescope. Last counter total absorption type. $ACCCCC_a$
number of counters	3	3	4	4	4	6	4	4	6
thickness of converter, cm	0.65 (Pb)	–	0.65 (Pb)	0.5 (Pb)	0.5 (Pb)	0.5 (Pb)	0.23 (Pb)	0.23 (Pb)	0.62 (Pb)
thickness of absorber, cm	1.25 (C)	–	1.25–2.5 (C) or 5.0 (Be)	–	7.0 (paraffin)	5.0 (paraffin)	15.0 (Be)	7.5 (Be)	5.7 (C)
thickness of intermediate absorber, cm	2.0 (Al)	–	2.0 (Al)	2.0 (Al)	2.0 (Al)	–	–	–	–
Efficiency of anticoincidence counter, %	98	–	98	–	–	99	98	98	98
Method of determining efficiency of telescope					From detectability of Compton-scattered γ's	In tagged photon beam	In bremsstrahlung beam with intensity reduced by 10^5 times	In bremsstrahlung beam with intensity reduced by 10^5 times	In bremsstrahlung beam with intensity reduced by 5×10^5 times
Hydrogen target:	In beam of monochromatic electrons and in bremsstrahlung beam	–	In beam of monochromatic electrons and in bremsstrahlung beam	–					
type	Polystyrene foam container	Polystyrene foam container	Polystyrene foam container	Polystyrene foam container	Polystyrene foam container with liquid-nitrogen jacket	Mylar appendix (75 μm) perpendicular to beam	Metallic appendix perpendicular to beam	Metallic appendix perpendicular to beam	Metallic appendix oriented along the beam
dimensions, cm	$d = 12.5$	–	$d = 12.5$	–	$d = 120; l = 30$	$d = 7.3$	$d = 10$	$d = 10.0; h = 12.5$	$d = 7.2; l = 50.0$
Counting rate of effect, counts/h	60	–	60	–	30–60	60	7	60	10
Ratio of counting rate with and without hydrogen	1.5	–	–	–	2–4	2	2–3	–	5–6
Results of experiment:									
energy range, MeV	25–95	30–90	25–87	75–119	40–70	55–120	50–130	50–130	70–123
number of experimental points	6	4	4	3	6	9		9	3
absolute error, %	8	–	8	–	6	1	7	10	–
relative error, %	8	8	5	10					

photons from the elastic scattering of γ's at low energies, a telescope of scintillation counters was used in Ref. 32. The layout of the experimental apparatus of Ref. 32 is shown in Fig. 1.

The telescope consists of four scintillation counters with plastic scintillators up to 2.1 g/cm^2 thick placed inside thin-wall aluminum containers, a lead converter (4.8 g/cm^2 thick), an interchangeable carbon absorber, and a laminated scintillation counter $C^+(A^+)$. The first scintillation counter (A) was connected in anticoincidence, and the next three in coincidence. This telescope is distinguished from the others usually used to detect γ's at energies $\lesssim$100 MeV by the fact that the last (laminated) counter is connected simultaneously to the coincidence and anticoincidence circuits. Its connection to the latter makes it possible to restrict the range of γ detection at high energies.

The detection range is restricted at low energies by means of additional absorbers placed in front of the first three counters connected in coincidence. Thus, one can detect γ's in a definite energy range, which is characterized by the thickness of the material placed in front of counters 4 and $C^+(A^+)$. The straggling of electron ranges due to fluctuations in the bremsstrahlung energy loss leads to a significant spreading of the detection interval.

To define the γ detection interval more precisely, the last (anticoincidence) counter must have a high γ detection efficiency. In Ref. 32, the anticoincidence counter

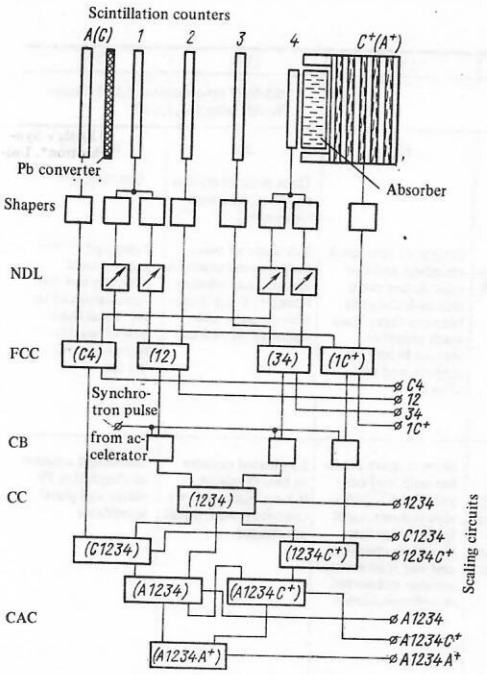

FIG. 1. Block diagram of experimental apparatus[32] for investigating Compton scattering on the proton at energies from 50 to 120 MeV: $A(C)$, 1, 2, 3, 4, $C^+(A^+)$ are scintillation counters; NDL are nanosecond delay lines; FCC are fast coincidence circuits; CC and CAC are coincidence and anticoincidence circuits; CB is the control block.

consisted of a cylindrical housing, a plastic scintillator with external diameter 20 cm, internal diameter 17 cm, and length 10.4 cm, and a laminated radiator of diameter 20 cm having six plastic scintillators: two 2 cm thick and four 0.5 cm thick, and five disks of TF-1 lead glass 1 cm thick.

To obtain a high accuracy in the measurement of the differential cross sections of γ elastic scattering on protons (about 1%) using just the one experimental apparatus of Ref. 32, two processes were observed successively on a hydrogen target in identical energy ranges: elastic scattering of γ's on electrons and on protons. The cross section of the control Compton scattering on electrons was calculated with an error of about 1% by the Klein–Nishina–Tamm expression, corrections for the double Compton effect and radiative corrections being introduced.

The evaluation of the experimental data by a "direct" absolutization and by the relative measurement through the control process led to results that agreed to within the accuracy of the absolutization of the experimental data. The calculation of the cross section by means of the relative measurements through the control process makes it possible to eliminate many systematic errors inherent in methods of direct absolutization resulting from errors in the measurement of the flux, the profile of the bremsstrahlung spectrum, the absolute values of the detection efficiency, etc.

The geometry of the experiment of Ref. 32 for the elastic scattering of γ's on protons in the range from 70 to 110 MeV is shown in Fig. 2. This indicates the position of the γ telescope for measuring the cross section of elastic scattering of the γ's on protons for the angle 90% and its position for the control experiment at the angle 1°47′. In the experiments described in Ref. 32, a liquid-hydrogen target was used; this consisted of a thin-wall (Mylar 75 μm thick), vertically suspended cylindrical vessel of diameter 7.3 cm. In the experiments, a comparatively small target was used—about 10 times smaller than the targets used in the earlier investigations Refs. 8 and 9 into the elastic scattering of γ's at low energies. The small size of the target made it possible to avoid the introduction of corrections for multiple background processes in the target itself. In addition, the small size of the target appreciably reduced the indeterminacy in calculation of the effective number of nuclei of the target at different angles of detection of the γ's from the process (1). The fairly thin walls of the cylindrical vessel made it possible to obtain a satisfactory effect/background ratio, the values of which are given in Table 3.

With regard to the results of experimental studies, we must make special mention of the work carried out at the P. N. Lebedev Physics Institute. Observations of the Compton effect on the proton are reported in Ref. 13, while the coefficients of the electrical and magnetic polarizability of the proton were determined for the first time in Ref. 9.

The experimental data obtained at the University of Chicago are given in Ref. 12, which probably includes the results of earlier investigations of the same authors.[10,11] The differential cross sections corresponding to angles 50, 60, and 70° and corrected for multiple background processes are indicated by an arrow in Table 1. These corrections were made by Oxley and Telegdi in Ref. 10.

The results obtained at MIT in Ref. 33 were later re-evaluated by the authors[34] but have not yet been published, and therefore the results of Ref. 33 are not given in Tables 1 and 2.

Three experimental points obtained at the University of California[14] contain a large indeterminacy in the absolute value of the cross section due to the errors associated with determining the efficiency of the γ telescope; we have already discussed these errors. In Table 1, we give the results of Ref. 14 normalized

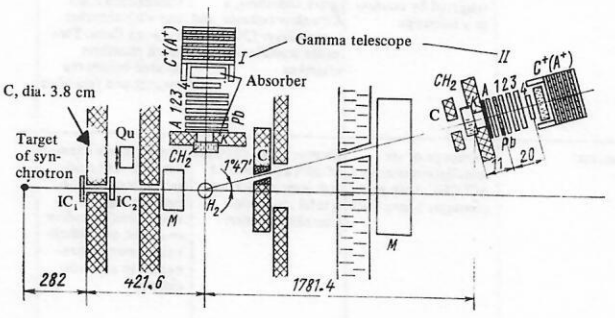

FIG. 2. Geometry of the experiment[32] to investigate Compton scattering on the proton in the energy range 70–110 MeV: C is the collimator, IC_1 and IC_2 are thin-wall ionization chambers; Qu is the quantameter; M is the sweeping magnet; A, 1, 2, 3, 4, $C^+(A^+)$ are scintillation counters; H_2 is the hydrogen target.

TABLE IV.

Experimental paper	[21]	[22]	[27]	[30]	[31]	[18]	[20]
Characteristics, type of accelerator	Betatron*, University of Illinois, USA			Synchrotron, Cornell University, USA		265-MeV synchrotron, P.N. Lebedev Physics Institute, USSR	
Maximal energy, MeV	300	335	1200	1300	1300	265	230—264
Monitoring of γ beam	Thick-wall ionization chamber, calorimeter	Quantameter	Quantameter	—	—	Thick-wall ionization chamber. Reaction $^{12}C(\gamma,n)^{11}C$	Quantameter
Proton detector:	Magnetic spectrometer and telescope of two scintillation counters. Chamber with He located between poles of magnet. Entry window Mylar, 75-μm thick	Magnetic spectrometer and system of two scintillation counters and four spark chambers	Telescope of four scintillation counters. Limits of detection intervals specified by range by connection of counters in coincidence	System of three scintillation counters and three track spark chambers in a constant magnetic field	System of four spark chambers and two scintillation counters with absorber between them. Two spark chambers located before the magnet, and two after it	Telescope of three proportional counters and one scintillation counter. Total thickness of matter, reduced to Al: 0.3 cm	Telescope of five proportional counters and one scintillation counter. Total thickness of matter, reduced to Al: 0.1 cm
Gamma detector: type	1. Total absorption Čerenkov counter made of cylindrical blocks of lead glass (two blocks) 2. Block of lead glass immersed in a container with water	System of alternating Pb plates (0.62 cm thick), spark chambers (6 layers), and plastic scintillators (1.25-cm thick). Two sets	1. Čerenkov counter 2. Scintillation counter connected in anticoincidence	System of a spark chamber with lead converter (1.96 rad. lengths), scintillation counter, Čerenkov counter, and shower spark chamber with lead plates; total thickness 4 rad. lengths	Shower spark chamber with lead converter and scintillation counter, eight total-absorption Čerenkov counters, and one scintillation counter connected in anticoincidence	Laminated counter of two Pb plates 0.8-cm thick and two containers with liquid scintillator	Laminated counter of alternating Pb plates and plastic scintillator
dimensions, cm	1. $d=22.8$ $l=20.3$ 2. $d=22.8$ $l=20.3$	—	1.38×38	—	—	—	Thickness 3.3—5.0 rad. lengths
Method of determining efficiency	In beam of monochromatic electrons	—	—			In monochromatic beam of γ's from decay of neutral pions	In monochromatic beam of γ's from decay of neutral pions
Hydrogen target: type	Mylar (38 μm) container for liquid hydrogen Lens-shaped	Mylar cylindrical container (75 μm)	Cylindrical container oriented perpendicular to beam	Cylindrical container		Brass (15 μm) appendix oriented perpendicular to beam	Cylindrical container oriented perpendicular to beam
dimensions, cm	$d=10.2$	$d=3.8$	$d=5.7$	—	—	$d=5.0$	$d=5.0$
Counting rate, counts/h	—	—	—	4000	—	3—10	3—10
Results of experiment:	120—282	210—310	300—750	480—1420	568—1890	235—250	213—249
energy range, MeV	17	5	8	28	43	6	10
number of points	10	—	15	10	—	15	20
absolute error, %	10—20	10—20	10	12	10—15	10	10
relative error, %							

Experimental paper	[17]	[7]	[31]	[29]	[24]	[42]	[25, 26, 28]
Characteristics, type of accelerator	P.N. Lebedev Physics Institute synchrotron, USSR	MIT synchrotron, USA		Synchrotron of Tokyo University, Japan		National Laboratory synchrotron, Frascati, Italy	Synchrotron of Bonn University, West Germany
Maximal energy	227	900	2000	700	1300	1000 (proton beam polarized at 320 MeV)	446
Monitoring of γ beam	Quantameter. Reaction $^{12}C(\gamma,n)^{11}C$	Quantameter	—	Quantameter	Thick-wall ionization chamber	Quantameter	Quantameter
Proton detector	Time-of-flight spectrometer. Start signal triggered by counter in γ telescope	System of three scintillation counters, two spark chambers, a Čerenkov counter, and a multilayer (30-plate) range scintillation chamber	System of four spark chambers and two scintillation counters with absorber between them. Two spark chambers located before the magnet and two after it	System of four scintillation counters (1 cm) and three spark chambers. Two four-layer chambers for determining the direction and one range chamber of 15 Al plates (0.3 cm)	System of four thin-wall spark chambers in a constant magnetic field, three scintillation counters, and a range spark chamber with 24 graphite plates (1.5 cm)	System of three scintillation counters and three spark chambers. Two chambers serve to measure the direction of the particle and one to measure the range of the protons	Range telescope of three scintillation counters. Two of them are specific-ionization counters
γ detector: type	Telescope of six scintillation counters, ACCCGC, with lead converter 5-mm thick	Shower spark chamber of 20 Ta plates 0.11 rad. length thick and a total absorption Čerenkov counter	Shower spark chamber with lead converter, scintillation counter, eight total absorption Čerenkov counters, one scintillation counter connected in anticoincidence	Five shower spark chambers with walls of brass (3 mm each) and aluminum (3 mm each)	Hodoscope of scintillation counters with Pb converter 0.5-cm thick and a total absorption Čerenkov counter	System of three scintillation anticoincidence counter, shower spark chamber with Pb plates 1.7 rad. lengths thick, and a total-absorption Čerenkov counter	Laminated counter of alternating Pb plates and plastic scintillator. Before the laminated counter an anticoincidence counter.
dimensions, cm		—	—	Thickness 4.4 rad.	—	—	Thickness 10 rad. lengths

Continuation of Table IV

Experimental paper	[17]	[7]	[31]	[29]	[24]	[42]	[25, 26, 28]
Characteristics, type of accelerator	P.N. Lebedev Physics Institute synchrotron, USSR	MIT synchrotron, USA		Synchrotron of Tokyo University, Japan		National Laboratory synchrotron, Frascati, Italy	Synchrotron of Boon University, West Germany
Method of determining efficiency	In beam of tagged protons	—	—	Monte Carlo calculation	—	—	—
Hydrogen target: type	Cylindrical container oriented perpendicular to the beam	—	—	Cylindrical container oriented perpendicular to beam	Cylindrical container	Cylindrical container oriented along beam	Cylindrical container oriented perpendicular to beam
size, cm	$d=7.3$	—	—	$d=3.0$	$d=3.0$	$l=15$	$d=6.0$
Counting rate, counts/h	—	900	—	70—650	—	—	—
Results of experiment:							
energy range, MeV	180—210	535—832	870—1890	314—692	700—800	300—335	237—430
number of points	3	11	21	9	2	1	25
absolute error, %	8	—	—	5	—	—	5
relative error, %	15	8	10—15	25	70	20	10

in accordance with Powell's cross section[35] at energy 70 MeV. This normalization, made in Ref. 14, corresponds to a reduction of the measured cross sections by 24%. In Table 2, the results of Ref. 14 are given without modification. The absolute errors of the experimental data, associated with inaccuracies in the determination of the bremsstrahlung flux and in the determination of the efficiency of the γ counters, are given in Tables 3 and 4. Only in Refs. 8, 13, and 14 are the errors in the absolute values of the cross sections not given.

Experiments in the Energy range 120—400 MeV. The elastic scattering of γ's on protons in the energy range 120—300 MeV has been investigated at the University of Illinois, USA, [21,22] at the P. N. Lebedev Physics Institute, [18–20] and at the University of Bonn in West Germany. [25,26,28] The main characteristics of the experimental apparatus used at energies above the pion photoproduction threshold are given in Table 4.

In Ref. 21, the recoil protons were analyzed according to their momenta by means of a magnetic spectrometer and were observed by means of a telescope of two scintillation counters that measured the specific energy loss and the total energy of the proton. The γ's were observed by means of a total absorption Čerenkov counter with a radiator of lead glass. The energy resolution of such a counter for 150-MeV γ's is ± 25%. In the investigation Ref. 22, which was made several years later, an appratus was used with not only scintillation counters but also spark chambers to observe the protons and γ's. In Refs. 21 and 22, experimental data corresponding to the energy dependence of the cross section at the angle 90° in the energy range 120—240 MeV are given.

In Refs. 18—20, detailed investigations were made of the angular distribution of the differential cross section of elastic scattering of γ's on protons at 214 and 249 MeV. When the process (1) is investigated by observing coincidences between the recoil proton and the scattered γ, the range of angles accessible to experimental investigation is restricted at small angles of emission of the protons by the increase in the general background loading on the counters and at large emission angles by the minimal ranges of the protons that can still be detected by the apparatus. The detection ranges for the elastic scattering of γ's for the two maximal energies 230 and 264 MeV of the bremsstrahlung spectrum are given in Fig. 3. It can be seen from this figure that in these ranges of angles and energies only protons from elastic scattering on hydrogen are detected, and not recoil protons from pion photoproduction.

In Refs. 18—20, a telescope of proportional counters was used to detect protons. In Ref. 20, the amount of matter in the path of the protons was reduced by use of a telescope of proportional counters with wire cathodes, and a scintillation counter with scintillator as thin as 0.1 mm was used to obtain fast $p\gamma$ coincidences. The

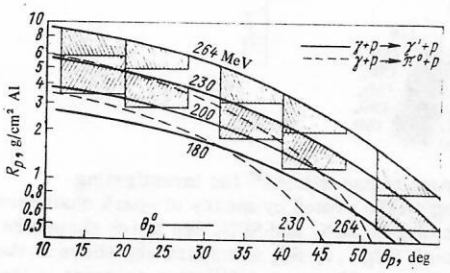

FIG. 3. Regions of detection of Compton scattering on protons at energies above the pion-photoproduction threshold: θ_p is the angle of emission of the recoil proton; R_p is the range of the recoil proton.

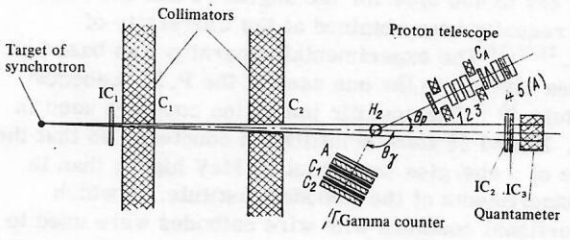

FIG. 4. Geometry of experiments[20] to investigate Compton scattering on the proton in the energy range 200—250 MeV: C_1 and C_2 are collimators of the γ beam; IC_1, IC_2, IC_3 are thin-wall ionization chambers; 1, 2, 3, 4, 5(A) are proportional counters with wire cathodes; A, C_1, C_2, C_p are scintillation counters.

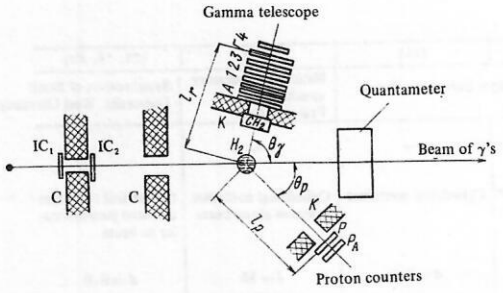

FIG. 5. Geometry of experiment[17] for investigating Compton scattering on the proton in the energy range 130—220 MeV: C is the collimator; IC_1, IC_2 are thin-wall ionization chambers; A,1,2,3,4,Γ,P,P_A are scintillation counters; H_2 is the hydrogen target.

geometry of this experiment is shown in Fig. 4. The telescope for detecting the recoil protons is positioned at the angles 16, 24, 36, 44, 56, and 64°. The γ counter is positioned at angles calculated in accordance with the kinematics of the elastic scattering process at 140, 121, 94, 78, 50, and 42°. The scattered γ's are detected by a laminated counter consisting of alternating layers of lead and scintillator. In Refs. 18 and 20, much attention was devoted to different types of background measurements, among which we should mention the experiments made with the γ counter at "incorrect" positions not corresponding to the correlated angles of emission of the recoil proton and the scattered γ. These experiments were made with a full and empty (vacuum) target, and also with an "incorrect" time delay in the channel of the γ counter. The main source of the background was random coincidences, whose counting rate was equal to the yield measured from a full hydrogen target but at an "incorrect" position of the γ counter. The background was 10—20% of the measured effect.

The results of the measurements made at 249 MeV (see Refs. 18 and 20) agreed satisfactorily with each other and were combined. These results were published in Ref. 20 and are given in Table 2. The errors in the determination of the differential cross sections given in Table 4 for the results of Refs. 18 and 20 include the statistical errors of the measured yields and the inaccuracies in calculating the cross sections by the Monte Carlo method.

A large number of data referring to the energy range from 237 to 430 MeV for the angles 90 and 110—130° have recently been obtained at the University of Bonn.[25,26,28] The experimental apparatus was based on an idea similar to the one used at the P. N. Lebedev Institute.[18,20] The specific ionization counters used in Refs. 26 and 28 were scintillation counters, so that the range of γ energies was about 20 MeV higher than in the experiments at the Lebedev Institute, in which proportional counters with wire cathodes were used to measure the specific ionization.

An investigation has recently been made at the Lebedev Institute[17] into the elastic scattering of γ's on protons at 90° in the center-of-mass system in the energy range 180—220 MeV with a time-of-flight spectrometer in the subnanosecond region for detecting the protons. A block diagram of the experiment is shown in Fig. 5. The synchrotron at the Institute (energy 265 MeV) was operated with a maximal bremsstrahlung energy 227 MeV. The telescope for detecting the γ's was placed at 76°. The recoil protons were observed by the counter P, which was placed at an angle of 47° with respect to the primary γ beam at a distance 105 cm from the center of the liquid-hydrogen target. The counter P_A, connected in anticoincidence to restrict the range of proton detection at high energies (to eliminate detection of energetic protons from the walls of the hydrogen target) was placed directly behind the counter P. The signals from the counters Γ (in the γ counter) and P were transmitted to the start and stop inputs of a time-to-pulse-height converter. The remaining counters in the experiment served to generate the controlling trigger signal.

To obtain a satisfactory statistical error, the complete range of detection with respect to the proton times of flight from 10 to 40 nsec was divided into individual groups in the process of evaluation of the experimental data; the width of the time interval in each of these groups was appreciably greater than the time resolution of the spectrometer, which was ± 0.3 nsec.

Background measurements were made with an empty target, and with a target filled with hydrogen but with the γ telescope at an "incorrect" position. The results of these two groups of background measurements agreed to within the statistical error and were combined. The level of the background was not more than 30% of the measured yield. The main characteristics of all the experimental equipment are given in Table 4. It can be

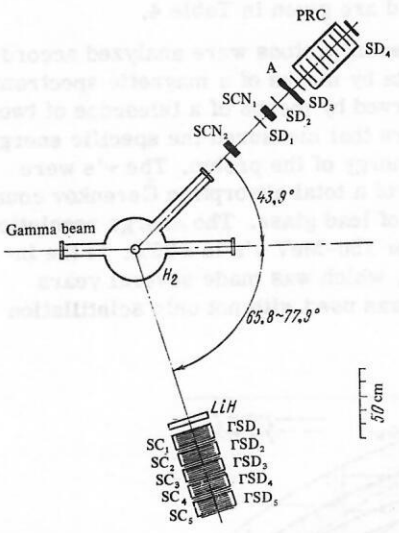

FIG. 6. Arrangement of experiment[29] for investigating Compton scattering on the proton by means of spark chambers: H_2 is the hydrogen target; SCN_1 and SCN_2 are spark chambers in the proton channel; $SC_1, \ldots, SC_5$ are spark chambers in the gamma channel; $SD_1, \ldots, SD_4$ are scintillation counters in the proton channel; PRC is the spark chamber for measuring the range of the recoil proton; A is an absorber; $\Gamma SD_1, \ldots, \Gamma SD_4$ are scintillation counters in the gamma channel; LiH is an absorber.

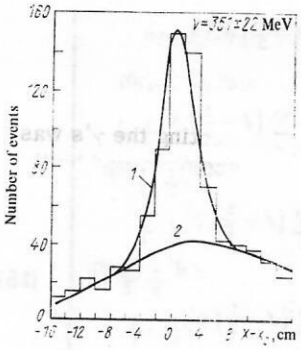

FIG. 7. Illustration of the possibility of kinematic separation of the reactions (1) and (2) by means of spark chambers in Ref. 29. 1) Is the observed number of $p\gamma$ coincidences; 2) the calculated number of $p\gamma$ coincidences from the reaction (2).

seen from Figs. 11–18 that the results of the measurements agree satisfactorily with one another.

Experiments at energies above 400 MeV. The characteristic feature of investigations of elastic scattering of γ rays at high energies is the use of spark chambers to observe the gammas and the recoil protons. By means of this method, one can determine the spatial coordinates of the particles and separate kinematically the elastic scattering in the smoothly varying background of pion photoproduction process. This method of identification of elastic scattering is used in the majority of investigations made at high energies.[7,24,29–31,36–39] The experiments made on the linear accelerator[40,41] at Stanford, in which the γ's had energy in the range 17–18 GeV, are an exception.

The main characteristics of the experimental apparatus are given in Table 4. The arrangement of the experiment at the University of Tokyo[29] with spark chambers is shown in Fig. 6. In this experiment, the protons were detected by scintillation counters and spark chambers, one of which was intended to determine the range of the protons. The scattered γ's were detected by five spark chambers and a system of five total-absorption counters. The use of the spark chambers made it possible to determine the angle of emission of the recoil proton and the scattered γ with sufficient accuracy and to distinguish kinematically the reactions (1) and (2). The possibility of such separation is demonstrated in Fig. 7, which gives the distribution of the number of events as a function of the angle (coordinate) of emission of the γ. The sharply peaked distribution (curve 1 in Fig. 7) corresponds to the correlation between the proton and the γ. The distribution of the background events resulting from the detection of protons and γ's from the reaction (2) is shown by curve 2.

Among the experiments made in the energy range from 400 MeV to 1.5 GeV we should mention the detailed measurements of the energy dependence of the cross sections at angle 90° made at Cornell University[30] and at MIT[7] at γ-ray energies up to 1450 MeV, and the dependence of the cross section on the square of the momentum transfer at small t values obtained in the accelerators at Stanford,[40,41] DESY,[26] and at MIT.[37] Measurements of the cross section in a beam of polarized γ's made at Frascati[42] and measurements of the polarization of the recoil protons made at the University of Tokyo are of undoubted interest.[24] However, these and other data, as can be seen from Table 2, have a low statistical accuracy.

2. KINEMATICS

We denote the four-momenta of the incident and scattered γ's by k_1 and k_2 and the corresponding momenta of the nucleons by p_1 and p_2. From these vectors one can form the invariants

$$\left.\begin{aligned} s&=(p_1+k_1)^2;\\ u&=(p_1-k_2)^2;\\ t&=(k_2-k_1)^2. \end{aligned}\right\} \tag{3}$$

These are related by

$$s+u+t=2m^2, \tag{4}$$

where m is the mass of the nucleon.

In the center-of-mass system of the s channel, the invariant variables s, u, and t have the form

$$\left.\begin{aligned} s&=W^2;\\ u&=m^2-2\omega(E+\omega\cos\theta);\\ t&=-2\omega^2(1-\cos\theta); \end{aligned}\right\} \tag{5}$$

where W is the total energy; $\omega=(s-m^2)/(2s^{1/2})$ is the γ energy; $E=(s+m^2)/(2s^{1/2})$ is the nucleon energy; and θ is the scattering angle. In this channel, s is the square of the total energy and t is the square of the momentum transfer.

In the center-of-mass system of the t channel

$$\left.\begin{aligned} s&=-2\tilde{p}^2-m^2+2\tilde{p}\tilde{E}\cos\psi;\\ u&=-2\tilde{p}^2-m^2-2\tilde{p}\tilde{E}\cos\psi;\\ t&=4\tilde{\omega}^2=4\tilde{E}^2. \end{aligned}\right\} \tag{6}$$

where $\tilde{\omega}$ is the energy of the γ; $\tilde{p}$ and $\tilde{E}$ are the momentum and energy of the nucleon; and Ψ is the scattering angle. Here we have $\cos\psi=(s-u)/4\tilde{p}\tilde{\omega}=(s-u)/[t(t-4m^2)]^{1/2}$. We represent the S matrix in the form

$$S_{fi}=\delta_{fi}+\frac{i\pi\delta(p_1+k_1-p_2-k_2)}{(2\pi)^2[4E_1E_2\omega_1\omega_2]^{1/2}}\bar{u}(p_2)T_{fi}u(p_1); \tag{7}$$

where ω_1 and ω_2 are, respectively, the energies of the initial and the final γ's; E_1 and E_2 are the energies of the initial and final nucleons.

To find the invariant structure of the amplitude T_{fi}, we introduce the following system of orthogonal basis vectors:

$$\left.\begin{aligned} K&=(k_1+k_2)/2;\\ Q&=(k_2-k_1)/2;\\ P'&=P-(PK)K/K^2;\ N_\mu=i\varepsilon_{\mu\nu\lambda\sigma}P'_\nu K_\lambda Q_\sigma, \end{aligned}\right\} \tag{8}$$

where $P=(p_1+p_2)/2$.

Then the requirements of parity conservation, gauge invariance, invariance under charge conjugation, and the condition of crossing symmetry enable one to write the amplitude T_{fi} in the form[43–45]:

$$\begin{aligned}\bar{u}(p_2)T_{fi}u(p_1)=-\bar{u}(p_2)\Big\{&\frac{(e_2P')(e_1P')}{(P')^2}[T_1+\hat{K}T_2]\\ &+\frac{(e_2N)(e_1N)}{N^2}[T_3+\hat{K}T_4]+\frac{(e_2P')(e_1N)-(e_2N)(e_1P')}{(P')^2K^2}\gamma_5T_5\\ &+\frac{(e_2P')(e_1N)+(e_2N)(e_1P')}{(P')^2K^2}\gamma_5\hat{K}T_6\Big\}u(p_1),\end{aligned} \tag{9}$$

where e_1 and e_2 are the polarization four-vectors of the initial and final γ's; the amplitudes T_i are functions of

only the invariant variables s, u, and t and have the following symmetry properties under the substitution $s \rightleftarrows u$:

$$T_i(s,t) = \eta_i T_i(u,t); \quad \eta_i = \begin{cases} 1 & \text{for } i = 1, 3, 5, 6 \\ -1 & \text{for } i = 2, 4. \end{cases}$$

The (cms) differential cross section for scattering of unpolarized γ's on a nucleon constructed by means of the invariant amplitudes T_i has the form

$$\begin{aligned} \frac{1}{r_0^2}\frac{d\sigma}{d\Omega} = \frac{1}{4e^4}\frac{m^2}{W^2}\{&(E^2+m^2-\omega^2 z)\cdot(|T_1|^2+|T_3|^2) \\ &+2W\omega^2(E+\omega z)(|T_2|^2+|T_4|^2) \\ &+2m\omega(2E+\omega+\omega z)\,\mathrm{Re}\,(T_1T_2^*+T_3T_4^*) \\ &+2\omega^2(1-z)|T_5|^2+2\omega^2W^2(1+z)|T_6|^2\}, \end{aligned} \tag{10}$$

while for the scattering of γ's polarized at angle φ to the scattering plane it is

$$\begin{aligned} \frac{1}{r_0^2}\frac{d\sigma}{d\Omega} = \frac{1}{2e^4}\frac{m^2}{W^2}\{&[(E^2+m^2-\omega^2 z)|T_1|^2 \\ &+2W\omega^2(E+\omega z)|T_2|^2+2m\omega(2E+\omega+\omega z)\,\mathrm{Re}\,T_1T_2^*]\sin^2\varphi \\ &+[(E^2+m^2-\omega^2 z)|T_3|^2+2W\omega^2(E+\omega z)|T_4|^2 \\ &+2m\omega(2E+\omega+\omega z)\,\mathrm{Re}\,T_3T_4^*]\cos^2\varphi \\ &+\omega^2(1-z)|T_5|^2+W^2\omega^2(1+z)|T_6|^2\}. \end{aligned} \tag{11}$$

where $r_0 = e^2/(4\pi m)$: $z = \cos\theta$.

In the case of scattering of γ's on an unpolarized target, the polarization of the recoil nucleons in the direction perpendicular to the scattering plane is expressed by[45]

$$P\frac{d\sigma}{d\Omega} = -\frac{E\omega^2\sin\theta}{32\pi mW}\,\mathrm{Im}\,(T_1T_2^*+T_3T_4^*). \tag{12}$$

The cms amplitude of scattering of γ's on a nucleon can frequently be represented conveniently in the form[46]

$$\begin{aligned} \bar{u}(p_2)T_{fi}u(p_1) = &(\mathbf{e}_2\mathbf{e}_1)R_1+(\mathbf{s}_2\mathbf{s}_1)R_2 \\ &+i(\sigma[\mathbf{e}_2\mathbf{e}_1])R_3+i(\sigma[\mathbf{s}_2\mathbf{s}_1])R_4 \\ &+i[(\sigma\varkappa_1)(\mathbf{s}_2\mathbf{e}_1)-(\sigma\varkappa_2)(\mathbf{s}_1\mathbf{e}_2)]R_5 \\ &+i[(\sigma\varkappa_2)(\mathbf{s}_2\mathbf{e}_1)-(\sigma\varkappa_1)(\mathbf{s}_1\mathbf{e}_2)]R_6, \end{aligned} \tag{13}$$

where

$$\mathbf{s}_1 = [\varkappa_1\mathbf{e}_1];\ \mathbf{s}_2 = [\varkappa_2\mathbf{e}_2];\ \varkappa_1 = \mathbf{k}_1/\omega;\ \varkappa_2 = \mathbf{k}_2/\omega.$$

These amplitudes R_i are related to the T_i's by

$$\begin{aligned} T_1 &= 2m\{-(W-m)(R_1z+R_2)+[(W+m)+(W-m)z]R_3\}/(W^2-m^2); \\ T_2 &= 2m\{-(W-m)^2(R_1z+R_2)-[(W+m)^2-(W-m)^2z]R_3\}/(W^2-m^2)^2; \\ T_3 &= 2m\{(W-m)(R_1+R_2z)-[(W+m)+(W-m)z]R_4\}/(W^2-m^2); \\ T_4 &= 2m\{(W-m)^2(R_1+R_2z)+[(W+m)^2-(W-m)^2z]R_4\}/(W^2-m^2)^2; \\ T_5 &= 2mW\{(1-z)(R_5-R_3)+R_3-R_4\}/(W^2-m^2); \\ T_6 &= 2m\{(1-z)(R_5+R_6)+R_3+R_4\}/(W^2-m^2). \end{aligned} \tag{14}$$

Let us consider the helicity amplitudes[45] for Compton scattering: $\langle\xi_2,\lambda_2|T|\xi_1,\lambda_1\rangle$, where $|\xi_1,\lambda_1\rangle$ denote the states with nucleon helicity ξ_i and γ helicity λ_i. The six linearly independent amplitudes and their partial-wave expansion can be written in the form

$$\begin{aligned} \phi_1 &\equiv \left\langle \tfrac{1}{2}, 1|T|\tfrac{1}{2}, 1\right\rangle = \frac{1}{\omega}\sum_J\left(J+\tfrac{1}{2}\right)\phi^J_{-1/2,\,-1/2}\times d^J_{-1/2,\,-1/2}(\theta); \\ \phi_2 &\equiv \left\langle -\tfrac{1}{2}, -1|T|\tfrac{1}{2}, 1\right\rangle = \frac{1}{\omega}\sum_J\left(J+\tfrac{1}{2}\right)\phi^J_{-\frac{1}{2},\,\frac{1}{2}}\times d^J_{-\frac{1}{2},\,\frac{1}{2}}(\theta); \\ \phi_3 &\equiv \left\langle \tfrac{1}{2}, -1|T|\tfrac{1}{2}, 1\right\rangle = \frac{1}{\omega}\sum_J\left(J+\tfrac{1}{2}\right)\phi^J_{-\frac{1}{2},\,\frac{3}{2}}\times d^J_{-\frac{1}{2},\,\frac{3}{2}}(\theta); \\ \phi_4 &\equiv \left\langle -\tfrac{1}{2}, 1|T|\tfrac{1}{2}, 1\right\rangle = \frac{1}{\omega}\sum_J\left(J+\tfrac{1}{2}\right)\phi^J_{-\frac{1}{2},\,-\frac{3}{2}}\times d^J_{-\frac{1}{2},\,-\frac{3}{2}}(\theta); \\ \phi_5 &\equiv \left\langle -\tfrac{1}{2}, 1|T|-\tfrac{1}{2}, 1\right\rangle = \frac{1}{\omega}\sum_J\left(J+\tfrac{1}{2}\right)\phi^J_{-\frac{3}{2},\,-\frac{3}{2}}\times d^J_{-\frac{3}{2},\,-\frac{3}{2}}(\theta); \\ \phi_6 &\equiv \left\langle \tfrac{1}{2}, -1|T|-\tfrac{1}{2}, 1\right\rangle = \frac{1}{\omega}\sum_J\left(J+\tfrac{1}{2}\right)\phi^J_{-\frac{3}{2},\,\frac{3}{2}}\times d^J_{-\frac{3}{2},\,\frac{3}{2}}(\theta). \end{aligned} \tag{15}$$

The amplitudes ϕ_i and T_i are related by

$$\begin{aligned} \phi_1 &= \cos(\theta/2)[m(T_3-T_1)+\omega W(T_4-T_2)-2\omega W T_6]; \\ \phi_2 &= -\sin(\theta/2)[E(T_1-T_3)+m\omega(T_2-T_4)-2\omega T_5]; \\ \phi_3 &= \cos(\theta/2)[m(T_1-T_3)+\omega W(T_2-T_4)]; \\ \phi_4 &= -\sin(\theta/2)[E(T_3-T_1)+m\omega(T_4-T_2)]; \\ \phi_5 &= \cos(\theta/2)[m(T_2-T_1)+\omega W(T_4-T_2)+2\omega W T_6]; \\ \phi_6 &= \sin(\theta/2)[E(T_1-T_3)-m\omega(T_2+T_4)+2\omega T_5]. \end{aligned}$$

The differential cross section for scattering of unpolarized γ's can be expressed in terms of the ϕ_i's:

$$\frac{d\sigma}{d\Omega} = \frac{1}{2}\frac{1}{64\pi^2 s}\{|\phi_1|^2+|\phi_2|^2+2|\phi_3|^2+2|\phi_4|^2+|\phi_5|^2+|\phi_6|^2\}.$$

The helicity amplitudes for γN scattering in the t channel have the form

$$\begin{aligned} \Sigma_1 &\equiv \left\langle 1, 1|T|\tfrac{1}{2}, \tfrac{1}{2}\right\rangle = \frac{1}{(\widetilde{p\omega})^{1/2}}\sum_J\left(J+\tfrac{1}{2}\right)G^J_{0,\,1}d^J_{0,\,0}(\psi); \\ \Sigma_2 &\equiv \left\langle 1, -1|T|\tfrac{1}{2}, \tfrac{1}{2}\right\rangle = \frac{1}{(\widetilde{p\omega})^{1/2}}\sum_J\left(J-\tfrac{1}{2}\right)G^J_{2,\,1}d^J_{2,\,1}(\psi); \\ \Sigma_3 &\equiv \left\langle -1, -1|T|\tfrac{1}{2}, \tfrac{1}{2}\right\rangle = \frac{1}{(\widetilde{p\omega})^{1/2}}\sum_J\left(J-\tfrac{1}{2}\right)G^J_{0,\,0}d^J_{0,\,0}(\psi); \\ \Sigma_4 &\equiv \left\langle 1, -1|T|\tfrac{1}{2}, -\tfrac{1}{2}\right\rangle = \frac{1}{(\widetilde{p\omega})^{1/2}}\sum_J\left(J-\tfrac{1}{2}\right)G^J_{2,\,1}d^J_{2,\,1}(\psi); \\ \Sigma_5 &\equiv \left\langle -1, 1|T|\tfrac{1}{2}, -\tfrac{1}{2}\right\rangle = \frac{1}{(\widetilde{p\omega})^{1/2}}\sum_J\left(J+\tfrac{1}{2}\right)G^J_{-2,\,1}d^J_{-2,\,1}(\psi); \\ \Sigma_6 &\equiv \left\langle 1, 1\ T|\tfrac{1}{2}, -\tfrac{1}{2}\right\rangle = \frac{1}{(\widetilde{p\omega})^{1/2}}\sum_J\left(J+\tfrac{1}{2}\right)G^J_{0,\,1}d^J_{0,\,1}(\psi). \end{aligned}$$

These amplitudes Σ_i are related to the T_i's by

$$\begin{aligned} \Sigma_1 &= \widetilde{p}(T_1+T_3)+\widetilde{\omega}m\cos\psi(T_2+T_4)+2\widetilde{\omega}T_5; \\ \Sigma_2 &= \widetilde{p}(T_3-T_1)-\widetilde{\omega}m\cos\psi(T_2-T_4); \\ \Sigma_3 &= \widetilde{p}(T_1+T_3)+\widetilde{\omega}m\cos\psi(T_2+T_4)-2\widetilde{\omega}T_5; \\ \Sigma_4 &= -\widetilde{\omega}^2\sin\psi(T_4-T_2)+2\widetilde{p\omega}\sin\psi T_6; \\ \Sigma_5 &= -\widetilde{\omega}^2\sin\psi(T_4-T_2)-2\widetilde{p\omega}\sin\psi T_6; \\ \Sigma_6 &= -\sin\psi\widetilde{\omega}^2(T_2+T_4). \end{aligned}$$

We expand the amplitudes R_i with respect to partial waves.[47] To this end, we introduce a notation for the partial-wave amplitudes of electric, E, and magnetic, M, transitions: $f^{L\pm}_{EE}$, $f^{L\pm}_{MM}$, $f^{L\pm}_{ME}$. Here, $f^{L\pm}_{EE}$ and $f^{L\pm}_{MM}$ are the amplitudes of Compton scattering of a γ with angular

momentum L and total angular momentum of the γN system $J = L \pm \frac{1}{2}$. As a result, the function R_i can be represented in the form

$$
\begin{aligned}
R_1 &= f^1_{EE} + 2f^-_{EF} + 2zf^2_{EE} - f^-_{MM} + 6zf^2_{EE};\\
R_2 &= f^1_{MM} + 2f^+_{MM} + 2zf^3_{MM} - f^2_{EE} - 3f^2_{EE};\\
R_3 &= f^1_{EE} - f^+_{EE} + 2zf^2_{EE} + f^3_{MM}/2 - 4zf^2_{EE} + 2\sqrt{3}\, f^+_{EM};\\
R_4 &= f^1_{MM} - f^+_{MM} + 2zf^2_{MM} + f^2_{EE}/2 - f^2_{EE} + 2\sqrt{3}\, f^+_{ME};\\
R_5 &= -f^2_{EE} - 2\sqrt{3}\, f^+_{ME} + 2f^2_{EE};\\
R_6 &= -f^2_{MM} - 2\sqrt{3}\, f^+_{EM}.
\end{aligned}
$$

The unitarity of the S matrix enables us to express the imaginary parts of the γN scattering amplitudes in terms of the amplitudes of photoabsorption on the nucleon. If we restrict ourselves to photoproduction of single pions, we obtain an expression for the partial waves of γp scattering in terms of the photoproduction partial waves:

$$
\begin{aligned}
&\operatorname{Im} f^1_{EE} = \nu_0 |E_{0+}|^2; \quad \operatorname{Im} f^-_{MM} = \nu_0 |M_{1-}|^2;\\
&\operatorname{Im} f^2_{EE} = \nu_0 |E_{1+}|^2; \quad \operatorname{Im} f^-_{MM} = \nu_0 |M_{2-}|^2;\\
&\operatorname{Im} f^+_{EE} = \nu_0 |E_{2-}|^2; \quad \operatorname{Im} f^+_{MM} = \nu_0 |M_{1+}|^2;\\
&\operatorname{Im} f^2_{EE} = \nu_0 |E_{3-}|^2; \quad \operatorname{Im} f^+_{ME} = \nu_0 \operatorname{Re} M_{1+} E^*_{1+};\\
&\operatorname{Im} f^+_{EM} = \nu_0 \operatorname{Re} E_{2-} M^*_{2-}.
\end{aligned}
\tag{16}
$$

Here, $\nu_0 = mq/(8\pi W)$, where q is the cms pion momentum. The photoproduction partial waves in (16) are related as follows to the multipole photoproduction amplitudes with definite values for the isospin and total angular momentum:

a) for production of π^+ mesons

$$
\begin{aligned}
E^{(+)}_{l\pm} = \sqrt{2}\,[&-E_{3J}\exp(i\alpha_{3J}) + E_{1J}\exp(i\alpha_{1J})]/3\\
&\mp \sqrt{2}\, A_S \exp(i\alpha_{1J});
\end{aligned}
$$

b) for production of π^0 mesons

$$
E^{(0)}_{l\pm} = [2E_{3J_1}\exp(i\alpha_{3J}) \mp E_{1J}\exp(i\alpha_{1J})]/2 + A_S \exp(i\alpha_{1J}).
$$

3. DISPERSION RELATIONS FOR THE γN SCATTERING AMPLITUDES

Introduction

Dispersion relations for forward Compton scattering amplitudes were considered for the first time by Gell-Mann, Goldberger, and Thirring[48]; using the causality condition, they arrived at the Kramers–Kronig dispersion relation.[49]

Dispersion relations for the amplitudes of γN scattering through an arbitrary angle were first proposed by Bogolyubov and Shirkov.[50] Rigorous proof of a dispersion relation for Compton scattering on a nucleon through any angle in the e^2 approximation was given by Logunov and Isaev,[51] who used the method proposed by Bogolyubov.[52]

Oehme and Taylor,[53] using local commutativity and spectral conditions, proved the validity of dispersion relations for Compton scattering on the nucleon under the condition that the square of the momentum transfer t lie in the range $0 \geqslant t > -12\mu^2$.

Let us now consider the papers in which Compton scattering on the nucleon has been analyzed on the basis of dispersion relations. The first numerical estimates were made in Ref. 48. Cini and Stroffolini[54] analyzed the dispersion relations for the scattering amplitudes of γ's polarized parallel and antiparallel with the proton spin and obtained the energy dependence of the differential cross section at angle 0°.

Capps,[55] analyzing the dispersion relations given in Ref. 48 for the scattering amplitudes of γ's polarized parallel and antiparallel with the proton spin and also using the dispersion relations obtained by Mathews,[56] constructed the differential cross sections of γp scattering for arbitrary angle. In the expansion of the amplitude, he restricted himself to a minimal number of partial waves.

Mathews[56] considered six independent amplitudes in the Breit coordinate system. He expanded these amplitudes in a series in the square of the momentum transfer and omitted the terms with degree higher than unity. For the coefficients of the expansion he wrote down subtracted dispersion relations. The scattering amplitudes contained 22 unknown subtractional constants, 12 of which were found by Mathews from the low-energy limit. He used the Born approximation to determine the remaining ten. The resulting dispersion relations were analyzed in the static limit. In the numerical analysis of the dispersion relations, contributions from the S wave (E_{0+}) and the first resonance (M_{1+}) of the amplitude of pion photoproduction on the proton were retained in the imaginary part of the scattering amplitude. In the same paper, Mathews showed that it is necessary to write down subtracted dispersion relations to achieve consistency with the low-energy limit.

Akiba and Sato[57] constructed six noncovariant amplitudes and wrote down dispersion relations for them, ignoring recoil. Expanding these amplitudes with respect to partial waves and restricting themselves to total angular momentum $J \leqslant \frac{3}{2}$, they obtained a system of relations for the partial waves. From these partial waves, they constructed the differential cross section of γp scattering at any angle. In the calculation of the imaginary part they took into account the contributions from E_{0+}, M_{1+}, and E_{1+}, the partial-wave amplitude E_{1+} being taken equal to M_{1+} or 0. Perturbation theory was used to find some of the subtractional constants.

Lapidus and Chou Kuang-Chau[44,58] used dispersion relations for a combination of the covariant amplitudes at 0°. Expressing these amplitudes in terms of partial waves, they obtained a system of relations for the partial waves with $J \leqslant \frac{3}{2}$. They showed that allowance for pion photoproduction in the S state[44] leads to the appearance of cusps in the energy dependence of the amplitudes and cross sections near the threshold.

The numerical results obtained in the above papers do not agree with the experimental data obtained for γ's with incident energy 180–220 MeV for the energy dependence of the differential cross sections for scattering through $\theta = 90$ and 135°. To eliminate this discrepancy, Jacob and Mathews[59] added the π^0 meson pole to the dispersion relations that Mathews had obtained earlier in Ref. 56. The possibility of this pole's making an important contribution to Compton scattering on the nucleon had been originally considered by Low. Jacob

and Mathews found that the best agreement with experiment is obtained for a π^0 meson lifetime of $\tau_{\pi^0}=10^{-18}$ sec. However, Lapidus and Chou Kuang-Chau[60] showed that if the π^0 meson decays into two γ's preferentially through a nucleon—antinucleon pair, as was considered in Ref. 61, it must contribute to the γ scattering amplitude on nucleons with a sign opposite to the one chosen by Jacob and Mathews. Therefore, in this case the discrepancy with experiment must be worse. To remove this discrepancy, Contogouris[62] took into account the two-pion isoscalar resonance with $J=0$; in addition, he considered the amplitude E_{1^+} and showed that its contribution may be important for energies above 250 MeV.

Using the dispersion relations of Jacob and Mathews,[59] Contogouris and Vergenelakis[63] considered simultaneously the two-pion resonance and the π^0 and η mesons. The π^0-meson residue was chosen with the same sign as in Ref. 60, and it was assumed that the η-meson residue enters with sign opposite to the residue at the π^0-meson pole, i.e., with a sign that decreases the differential cross section of Compton scattering on the proton in the region of low energies.

If Ref. 63, the energy dependence of the differential cross sections for scattering of unpolarized γ's and γ's polarized at $\theta=90°$ was investigated. For unpolarized γ's the two-pion resonance with $J=0$, $I=0$ and the η meson decrease the cross section, whereas for polarized γ's the two-pion resonance increases the cross section ratio $d\sigma_{\parallel}/d\sigma_{\perp}$ but the η meson decreases the ratio ($d\sigma_{\parallel}$ is the differential cross section for scattering of γ's polarized parallel with the scattering plane and $d\sigma_{\perp}$ is the perpendicular cross section).

Mueller[64] showed that the discrepancy with the experiment can be reduced by taking into account the contribution of the retardation term (π^+-meson pole in the photoproduction amplitude). Mueller used one-dimensional subtracted dispersion relations at fixed t. The dispersion relations were applied to the invariant amplitudes.

Note that in the majority of the investigations discussed here one-dimensional subtracted dispersion relations for the amplitudes of scattering through 0° were used. This is because the dispersion relations at fixed square of the momentum transfer t contain subtraction functions that depend on t. It is only for scattering angle $\theta=0°$ that these functions can be expressed in terms of the low-energy limit, whereas for nonzero scattering angle the subtraction functions remain unknown. The use of dispersion relations for the scattering amplitudes at 0° with subsequent recovery of the amplitude for any angle means that only a few partial waves can be taken into account in the scattering amplitudes. In the investigations in which dispersion relations were constructed for the scattering amplitudes at arbitrary angle it was assumed that the subtraction function is determined either simply by the low-energy limit[65] or by the low-energy limit in conjunction with the π^0-meson pole.[64]

The problem associated with finding the subtraction functions can be solved if one proceeds from double dispersion relations and constructs dispersion relations for the partial waves[66,67] or at fixed angle.[45] In these approaches, moreover, in contrast to the usual one-dimensional dispersion relations, contributions from the annihilation channel arise naturally and in a consistent manner. These problems can also be solved if to construct one-dimensional subtracted dispersion relations one uses simultaneously one-dimensional dispersion relations for different fixed invariant parameters. In what follows, we shall dwell in more detail on this last approach and on dispersion relations at fixed scattering angle.

Dispersion relations at fixed scattering angle

We consider the analytic properties of the scattering amplitude as a function of two complex variables. We assume that the scattering amplitude is an analytic function in the complete space of the two variables except for poles and cuts along certain hyperplanes. The position of the poles and the cuts with respect to the corresponding variable is determined by the unitarity condition for the scattering amplitude in the channel in which the given variable is the total energy. Applying Cauchy's theorem twice, we obtain double unsubtracted dispersion relations[68] for the amplitude of γ scattering on nucleons:

$$T_i(s,u,t)=\mathcal{P}_i+\frac{1}{\pi^2}\int\limits_{(m+\mu)^2}^{\infty}ds'\int\limits_{(m+\mu)^2}^{\infty}du'\times\frac{\rho_{12}(s'u')}{(s'-s)(u'-u)}+\frac{1}{\pi^2}\int\limits_{(m+\mu)^2}^{\infty}ds'\int\limits_{4\mu^2}^{\infty}\times\frac{\rho_{13}(s',t')}{t'-t}\left(\frac{1}{s'-s}+\frac{\eta_i}{s'-u}\right), \tag{17}$$

where μ is the pion mass; $\mathcal{P}_i$ are the single-nucleon poles and the π^0-meson pole;

$$\mathcal{P}_i=r_i[1/(m^2-s)+\eta_i/(m^2-u)]+\delta_i/(\mu^2-t). \tag{18}$$

In (18), r_i and δ_i have the form

$$\left.\begin{aligned} &r_1=-2e^2m(1+\tau_3)/2;\quad r_4=e^2[(1+\lambda_p)^2\times(1+\tau_3)/2+\lambda_n^2(1-\tau_3)/2];\\ &r_2=-e^2(1+\tau_3)/2;\quad r_5=e^2m(1+\lambda_p)\times(1+\tau_3)/2;\\ &r_3=0;\quad r_6=-e^2(1+\lambda_p)(1+\tau_3)/2;\end{aligned}\right\} \tag{19}$$

$$\left.\begin{aligned} &\delta_i=0\quad\text{for}\quad i\neq 5;\\ &\delta_5=\mu_{\pi^0}^2g_{\pi NN}F_\pi\tau_3/2;\ F_\pi=[64\pi\Gamma_{\pi^0\to 2\gamma}/\mu_{\pi^0}^3]^{1/2};\end{aligned}\right\} \tag{20}$$

where λ_p and λ_n are the anomalous magnetic moments of the proton and the neutron; $\Gamma_{\pi^0\to 2\gamma}$ is the $\pi^0\to 2\gamma$ decay width.

The imaginary parts of the amplitudes in the s and t channels are given by

$$A_i^{(s)}(s,t,u)=\operatorname{Im}T_i^{(s)}(s,u,t)=\frac{1}{\pi}\int\limits_{(m+\mu)^2}^{\infty}du'\times\frac{\rho_{12}(u',s)}{u'-u}+\frac{1}{\pi}\int\limits_{4\mu^2}^{\infty}dt'\frac{\rho_{13}(t',s)}{t'-t}\quad\text{for}\quad s\geqslant(m+\mu)^2;$$

$$A_i^{(t)}(s,t,u)=\operatorname{Im}T_i^{(t)}(s,t,u)=\frac{1}{\pi}\int\limits_{(m+\mu)^2}^{\infty}ds'\rho_{13}(s',t)\times\left(\frac{1}{s'-s}+\frac{\eta_i}{s'-u}\right)\quad\text{for}\quad t\geqslant 4\mu^2.$$

We define the following functions:

$$A_i^{(s)}(x, y) = \frac{1}{\pi}\int\limits_{(m+\mu)^2}^{\infty} du' \frac{\rho_{12}(x,u')}{u'-u(x)} + \frac{1}{\pi}\int\limits_{4\mu^2}^{\infty} dt' \frac{\rho_{13}(x,t')}{t'-y} \quad (21)$$

for $x \geqslant (m+\mu)^2$

and

$$A_i^{(t)}(x, y) = \frac{1}{\pi}\int\limits_{(m+\mu)^2}^{\infty} ds' \rho_{13}(s', y)\left(\frac{1}{s'-x} + \frac{\eta_i}{s'-u(x)}\right) \quad (22)$$

$y > 4\mu^2$,

where

$$u(x) = x^{-1}[m^4 - (x-m^2)^2(1+\cos\theta)/2];$$
$$t(x) = -[(x-m^2)^2/2x](1-\cos\theta).$$

The definitions (21) and (22) are convenient for obtaining dispersion relations at fixed $\cos\theta$ in which the right- and left-hand cuts are separated. To obtain such dispersion relations, we apply the identity

$$\int \frac{f(x', y(x))}{x'-x-i\varepsilon}dx' \equiv \int \frac{f(x', y(x))\,dx'}{x'-x-i\varepsilon}$$
$$+ P\int \frac{f(x', y(x))}{x'-x}dx' - P\int \frac{f(x', y(x))\,dx'}{x'-x}$$

to the denominators in (17).

After identification of the different contributions, we obtain[45]

$$T_i(s, \cos\theta) = \mathcal{P}_i + \frac{1}{\pi}\int\limits_{(m+\mu)^2}^{\infty} ds' \frac{A_i^{(s)}(s', t(s'))}{s'-s}$$
$$+ \frac{2\eta_i}{\pi}\int\limits_{(m+\mu)^2}^{\infty} \frac{du'}{u_-(u')-u_+(u')}\left\{\frac{u_+(u')}{u_+(u')-s(1+\cos\theta)}A_i^{(s)}\left(u', t\left(\frac{u_+(u')}{1+\cos\theta}\right)\right)\right.$$
$$\left. - \frac{u_-(u')}{u_-(u')-s(1+\cos\theta)}A_i^{(s)}\left(u', t\left(\frac{u_-(u')}{1+\cos\theta}\right)\right)\right\} \quad (23)$$
$$+ \frac{2}{\pi}\int\limits_{4\mu^2}^{\infty} \frac{dt'}{t_-(t')-t_+(t')}\left\{\frac{t_-(t')}{t_+(t')-s(1+\cos\theta)}A_i^{(t)}\left(t', \frac{t_+(t')}{1-\cos\theta}\right)\right.$$
$$\left. - \frac{t_-(t')}{t_-(t')-s(1+\cos\theta)}A_i^{(t)}\left(t', \frac{t_-(t')}{1-\cos\theta}\right)\right\},$$

where

$$u_\pm(x) = m^2(1-\cos\theta) - x \pm \{[m^2(1+\cos\theta)-x]^2 - m^4\sin^2\theta\}^{1/2};$$
$$t_\pm(x) = m^2(1-\cos\theta) - x \pm \{[m^2(1-\cos\theta)-x]^2 - m^4(1-\cos\theta)^2\}^{1/2}.$$

Let us consider the structure of the singularities of the relation (23) in the s plane. The contribution from the right-hand cut $s \geqslant (m+\mu)^2$ is given by the first integral in (23). The denominators $u_+(u') - s(1+\cos\theta) = 0$ give cuts $-\infty \leqslant s \leqslant u_-(\cos\theta)$ and $0 \leqslant s \leqslant u_+(\cos\theta)$; here $u_\pm(\cos\theta) = u_\pm(m+\mu)^2/(1+\cos\theta)$. The cut $0 \leqslant s \leqslant u_+$ is called the physical crossing cut. If $4\mu^2 > 2m^2(1-\cos\theta)$, the third integral is taken along the real cut $-\infty \leqslant s \leqslant \tau_-(\cos\theta)$, $\tau_+(\cos\theta) \leqslant s \leqslant 0$, where $\tau_\pm(\cos\theta) = t_\pm(4\mu^2)/(1-\cos\theta)$. But if $4\mu^2 < t' < 2m^2(1-\cos\theta)$, then for $|s| = m^2$ the cut is complex, i.e., $(\mathrm{Re}s + i\,\mathrm{Im}s)(1-\cos\theta) = t_\pm(t')$ and $\mathrm{Re}s = m^2 - 4\mu^2/(1-\cos\theta)$, $\mathrm{Im}s = \pm[m^4 - (\mathrm{Re}s)^2]^{1/2}$. On the other hand, for $4\mu^2 < 2m^2(1-\cos\theta)$ the cut is real and goes along $-\infty \leqslant s \leqslant 0$. On the cut around the circle we set $s = m^2\exp(i\alpha)$, and then t has the form

$$t = 4m^2\sin^2(\theta/2)\sin^2(\alpha/2). \quad (24)$$

In the second integral in the interval $-\infty \leqslant s \leqslant u_-(\cos\theta)$ we must deal with the function $A_i^{(s)}(u', t)(u_-(\cos\theta)/[1+\cos\theta])$ for unphysical values of the scattering angle, so that the expansion of this function with respect to Legendre polynomials does not converge. Therefore, in the numerical analysis of the dispersion relations for fixed angle[69] we must, on the basis of the philosophy of nearest singularities, restrict ourselves to the contribution to this integral from only the physical crossing cut.

In the third integral, when an expansion with respect to partial waves in the t channel is used, one can calculate the contribution from only the part of the cut around the circle. This expansion converges for $-40° \lesssim \alpha \lesssim 40°$, which, in accordance with (24), enables one to take into account consistently only the contributions of the nearest singularities in t.

The dispersion relations (23) are written down without subtractions. These dispersion relations do not give the low-energy limit in explicit form for the amplitudes T_1, T_3, T_5, and T_6. Therefore, for the amplitudes T_i $(i = 1, 3, 5, 6)$ we write down dispersion relations at fixed scattering angle with one subtraction[45]:

$$T_i(s, \cos\theta) = T_i(m^2, \cos\theta) + \overline{\mathcal{P}}_i + \frac{s-m^2}{\pi}\int\limits_{(m+\mu)^2}^{\infty} ds' \frac{A_i^{(s)}(s', t(s'))}{(s'-m^2)(s'-s)}$$
$$+ \frac{2\eta_i}{\pi}(s-m^2)(1+\cos\theta)\int\limits_{(m+\mu)^2}^{\infty} \frac{ds'}{u_-(s')-u_+(s')}$$
$$\times\left\{\frac{u_+(s')A_i^{(s)}(s', t(u_+(s'),[1+\cos\theta]))}{[u_+(s')-s(1+\cos\theta)][u_+(s')-m^2(1+\cos\theta)]}\right.$$
$$\left. - \frac{u_-(s')A_i^{(s)}(s', t(u_-(s'),[1+\cos\theta]))}{[u_-(s')-s(1+\cos\theta)][u_-(s')-m^2(1+\cos\theta)]}\right\} + \frac{2}{\pi}(s-m^2) \quad (25)$$
$$\times(1-\cos\theta)\int\limits_{4\mu^2}^{\infty} \frac{dt'}{t_-(t')-t_+(t')}$$
$$\times\left\{\frac{t_+(t')A_i^{(t)}(t', t_+(t')[1-\cos\theta])}{[t_+(t')-s(1-\cos\theta)][t_+(t')-m^2(1-\cos\theta)]}\right.$$
$$\left. - \frac{t_-(t')A_i^{(t)}(t', t_-(t')/[1-\cos\theta])}{[t_-(t')-s(1-\cos\theta)][t_-(t')-m^2(1-\cos\theta)]}\right\},$$

where

$$\overline{\mathcal{P}}_i = \frac{(s-m^2)r_i\sin^2\theta}{2m^2[2m^2-(s-m^2)(1+\cos\theta)]} - \frac{(s-m^2)(1-\cos\theta)\delta_i}{\mu^2[2\mu^2 s + (s-m^2)(1-\cos\theta)]} \quad (26)$$

and

$$T_1(m^2, \cos\theta) = -e^2(1+\tau_3)(1-\cos\theta)/2m;$$
$$T_3(m^2, \cos\theta) = e^2[2\lambda_p(1+\tau_3)/2 + \lambda^2]/m;$$
$$T_5 = (m^2, \cos\theta)$$
$$= e^2[(2\lambda_p(1+\tau_3)/2 + \lambda^2) + (1+\lambda_p)(1+\tau_3)(1-\cos\theta)/2]/2m;$$
$$T_6(m^2, \cos\theta) = e^2[-\lambda^2 - (1+\lambda_p)(1+\tau_3)(1-\cos\theta)/2]/2m^2, \quad (27)$$
$$\lambda = \lambda_p(1+\tau_3)/2 + \lambda_n(1-\tau_3)/2.$$

Numerical calculations were made by Köberle[69] only for the unsubtracted dispersion relations (23). In the t channel he took into account the contribution of the π^0 meson and the contribution of the $\pi\pi$ interaction in the nonresonance model using the $\pi\pi$-interaction phase shift[70] in the resonance model as well. A discrepancy with the experiment in the region of 200 MeV (especially at 90°) and in the region of the resonance energy remained.

Subtracted dispersion relations at fixed t

The approach adopted in Refs. 45, 66, 67, and 69 can be characterized by the fact that the functions investigated in these cases have complicated analytic properties in the complex plane of the variable s. This leads to

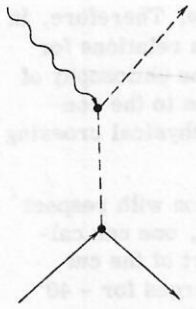

FIG. 8. Photoproduction diagram corresponding to exchange of π^+ mesons in the t channel.

additional assumptions when numerical calculations are made. These shortcomings can be avoided if for the amplitudes $T_i(s,u,t)$ one constructs one-dimensional subtracted dispersion relations for fixed $t \leq 0$ and uses one-dimensional dispersion relations at fixed u and the low-energy limit to find the subtraction functions.[71-76]

We shall assume that the amplitudes $T_i(s,u,t)$ $(i=1,3,5,6)$ satisfy the asymptotic conditions

$$T_i(s,t) \xrightarrow[t_{\text{fixed}}]{s\to\infty} s^{\alpha(t)}, \quad \alpha(t=0)\leqslant 1; \tag{28}$$

$$T_i(u,t) \xrightarrow[u_{\text{fixed}}]{t\to\infty} t^{\alpha(u)}; \tag{29}$$

$$T_i(u,s) \xrightarrow[u_{\text{fixed}}]{s\to\infty} s^{\alpha(u)}, \quad \alpha(u=m^2)<1. \tag{30}$$

These asymptotic conditions agree with the result given for the amplitudes T_i by Regge pole theory and the experimental data on $\alpha(u)$ (see Ref. 77).

The condition (28) enables one to write down for the amplitudes T_i a dispersion relation with respect to s and u for fixed $t \leq 0$ with one subtraction at the point u_0:

$$\begin{aligned}\operatorname{Re} T_i(s,u,t) &= r_i\left(\frac{1}{m^2-s}-\frac{1}{m^2-\bar{s}_0}\right)+r_i\left(\frac{1}{m^2-u}-\frac{1}{m^2-u_0}\right)\\ &+\frac{u-u_0}{\pi}P\int\limits_{(m+\mu)^2}^{\infty} ds' A_i^{(s)}(s',t)\left\{\frac{1}{(s'-u)(s'-u_0)}-\frac{1}{(s'-s)(s'-\bar{s}_0)}\right\}\\ &+\operatorname{Re} T_i(u_0,t),\end{aligned} \tag{31}$$

where $\bar{s}_0 = 2m^2 - u_0 - t$. For the amplitude $T_i(u_0,t)$ we write down a dispersion relation with respect to t and s for fixed $u_0 \leq m^2$ with one subtraction at the point $t_0 = 0$:

$$\begin{aligned}\operatorname{Re} T_i(u_0,t) &= r_i\left(\frac{1}{m^2-\bar{s}_0}-\frac{1}{m^2-\bar{s}_0(t=0)}\right)\\ &+\delta_i\left(\frac{1}{\mu^2-t}-\frac{1}{\mu^2-t_0}\right)+\frac{t}{\pi}P\int\limits_{4\mu^2}^{\infty}\frac{A_i^{(t)}(t',u_0)\,dt'}{t'(t'-t)}\\ &-\frac{t}{\pi}P\int\limits_{(m+\mu)^2}^{\infty}\frac{A_i^{(s)}(s',u_0)\,ds'}{(s'-\bar{s}_0)(s'-2m^2+u_0)}+\operatorname{Re} T_i(u_0,t_0=0).\end{aligned} \tag{32}$$

Substituting (32) into (31) and going to the limit $u_0 \to m^2$, we obtain[75,76]

$$\begin{aligned}\operatorname{Re} T_i(s,t) &= r_i\left(\frac{1}{m^2-s}+\frac{1}{m^2-u}\right)+\frac{\delta_i t}{\mu^2(\mu^2-t)}+T_i(m^2,0)\\ &+\frac{u-m^2}{\pi}P\int\limits_{(m+\mu)^2}^{\infty} ds' A_i^{(s)}(s',t)\left\{\frac{1}{(s'-m^2)(s'-u)}-\frac{1}{(s'-m^2+t)(s'-s)}\right\}\\ &+\frac{t}{\pi}\int\limits_{4\mu^2}^{\infty}\frac{A_i^{(t)}(t',u=m^2)}{t'(t'-t)}dt'-\frac{t}{\pi}P\int\limits_{(m+\mu)^2}^{\infty}\frac{A_i^{(s)}(s',u=m^2)\,ds'}{(s'-m^2)(s'-m^2+t)}.\end{aligned} \tag{33}$$

Here,

$$\left.\begin{aligned}&T_1(m^2,0)=0;\quad T_5(m^2,0)=e^2(2\lambda_p(1+\tau_3)/2+\lambda^2)/2m;\\ &T_3(m^2,0)=e^2(2\lambda_p(1+\tau_3)/2+\lambda^2)m;\quad T_6(m^2,0)=-e^2\lambda^2/2m^2.\end{aligned}\right\} \tag{34}$$

For amplitudes that are odd under the substitution $s \rightleftarrows u$, we can write down unsubtracted dispersion relations; they have the form

$$\begin{aligned}\operatorname{Re} T_j(s,t) &= r_j\left(\frac{1}{m^2-s}-\frac{1}{m^2-u}\right)\\ &+\frac{1}{\pi}P\int\limits_{(m+\mu)^2}^{\infty} ds' A_j^{(s)}(s',t)\left[\frac{1}{s'-s}-\frac{1}{s'-u}\right], \quad j=2,4.\end{aligned} \tag{35}$$

Let us consider here the physical assumptions made in the numerical calculation of the Compton scattering amplitudes in the framework of the dispersion relations (33) and (35). In the expansion of the imaginary part of the Compton scattering amplitude in the t channel with respect to intermediate states, allowance is made only for amplitudes corresponding to photoproduction of single pions on protons. In the photoproduction amplitudes, one retains the S wave (E_{0+}) and the partial waves that correspond to the first (M_{1+}), second (E_{2-}), and third (E_{3-}) resonances; each of these waves is assumed to be nonzero only in the range of energies corresponding to the resonance. When allowance is made for the "retardation" term (Fig. 8), one considers the main contributions associated with the quadratic function of this term and its interference with M_{1+} and E_{0+}. The partial waves E_{0+}, M_{1+}, E_{2-}, E_{3-} and the interference of E_{0+} with the retardation term are obtained by analyzing the experimental data on the photoproduction of pions on protons. This approximation to calculate the imaginary part of the Compton scattering amplitude in the s channel is sufficiently good for energies of the incident γ from 200 MeV up to the threshold of photoproduction of two pions.

In the range of γ energies from the single-pion photoproduction threshold (150 MeV) to 200 MeV nonresonance photoproduction multipoles may make an important contribution to the imaginary part of the Compton scattering amplitude. However, since the imaginary part of the scattering amplitude in this energy region is appreciably less than the real part, there are reasons for believing that neglect of the nonresonance photoproduction amplitudes leads to a small error (not more than 10%). Thus, the approximation can be regarded as admissible for the complete range of energies from 150 to 300 MeV.

A certain inaccuracy also arises from the neglect of the contribution from photoproduction of two or more

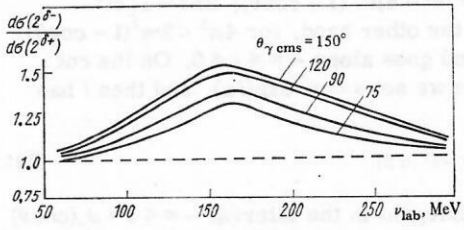

FIG. 9. Ratio of theoretical differential cross sections[73] with different signs of the residue δ for the π^0-meson pole as a function of the energy of the incident γ's.

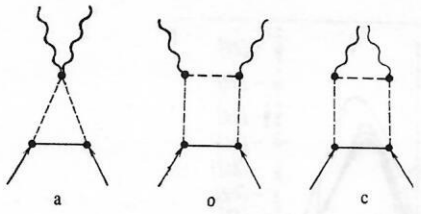

FIG. 10. Fourth-order Feynman diagrams that contribute to the t channel of γp scattering.

pions. This contribution is comparable with the contribution of the single-photoproduction multipoles responsible for the second and third resonances and does not exceed 10% for the range of incident γ energies up to 300 MeV.

In Ref. 78 it is shown that the predictions of γp scattering using different multipole analyses of the photoproduction[79–82] differ by not more than 10%.

Let us consider the procedure for taking into account the contributions to the γp scattering amplitude from the t channel. The nearest singularity in this channel is the π^0-meson pole, which is taken into account for $\delta_{\pi^0} > 0$ and $\delta_{\pi^0} < 0$. We recall that the sign $\delta_{\pi^0} > 0$ was first used in Ref. 59. To achieve agreement with the results of Ref. 61, in which it was assumed that the π^0 meson decays into two γ's through a nucleon-antinucleon pair, it is necessary to assume $\delta_{\pi^0} < 0$ (see Ref. 60). Allowance for the contribution of the π^0-meson pole with $\delta_{\pi^0} < 0$ increases the differential cross section in the range of energies we are considering. The ratio of the theoretical differential cross sections calculated in Ref. 75 with $\delta_{\pi^0} > 0 (\delta+)$ and $\delta_{\pi^0} < 0 (\delta-)$ is shown in Fig. 9 as a function of the energy of the incident γ for different fixed scattering angles. The strong dependence of the differential cross section of the Compton effect on the sign of the residue of the π^0-meson pole may be a justification for carrying out an analysis with a view to selecting, on the basis of the available experimental material, a variant of the theory and thus establishing what sign the π^0-meson pole residue does have.

In order to take into account the contribution of the η-meson pole, it is necessary to know the coupling constant of the η meson to the nucleon and the lifetime of the η meson. We take the coupling constant to be $g^2_{\eta NN}/4\pi \lesssim g^2_{\pi NN}/4\pi \approx 15$. (The bootstrap sum rules for NN scattering amplitudes[83, 84] give $g^2_{\eta NN}/4\pi \approx 1$.)

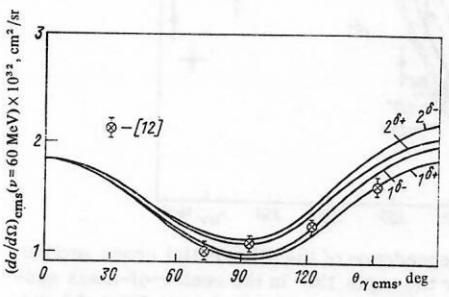

FIG. 11. Angular dependence of the differential cross section of γp scattering at 60 MeV: $1^{\delta-}$, $1^{\delta+}$, $2^{\delta-}$, $2^{\delta+}$ are the different variants of theoretical calculations.[73]

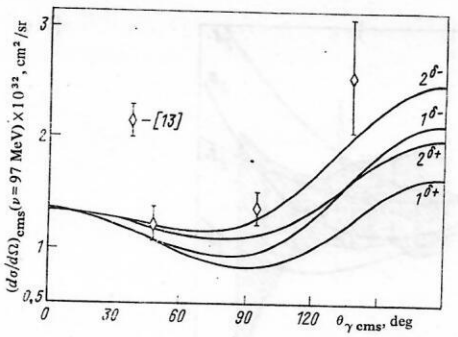

FIG. 12. Angular dependence of the differential cross section of γp scattering at 97 MeV: $1^{\delta-}$, $1^{\delta+}$, $2^{\delta-}$, $2^{\delta+}$ are the different variants of theoretical calculations.[73]

The experimental value of the $\eta \to 2\gamma$ decay width determined from the data of different experimental investigations fluctuates from 1.0 ± 0.23 keV in Ref. 85 to about 0.37 keV in Ref. 86. With these parameters, the η-meson pole makes a small contribution in this energy range to the γp differential scattering cross section and is therefore ignored in the numerical calculations.

Let us consider the procedure for taking into account the other intermediate states in the t channel. The contribution of these states can be estimated in two different theoretical calculations: In the first ($1^{\delta\pm}$) one takes into account in $A_i^{(t)}$ only two-particle states by means of the diagrams of fourth-order perturbation theory (Fig. 10); in the second ($2^{\delta\pm}$) one also uses the bootstrap model to take into account the contribution to $A_i^{(t)}$ of the states not considered in the first variant.[74–76] To this end, for the amplitude difference $T_i(s,t) - T_i(s,0)$ one constructs a dispersion relation first with respect to s and u for fixed t and then with respect to t and s for fixed u. These dispersion relations are then equated. As a result, the integral of $A_i^{(t)}$ can be expressed in terms of integrals of A_i^s as follows[76]:

$$\frac{t}{\pi} P \int_{4\mu^2}^{\infty} \frac{\bar{A}_i^{(t)}(t',\ u=m^2)\,dt'}{t'(t'-t)} = \frac{P}{\pi} \int_{(m+\mu)^2}^{\infty} ds' \left\{ [\bar{A}_i^{(s)}(s',t) - \bar{A}_i^{(s)}(s',0)] \left(\frac{1}{s'-m^2} + \frac{1}{s'-m^2+t} \right) + \frac{t\,[\bar{A}_i^{(s)}(s',\ u=m^2) - \bar{A}_i^{(s)}(s',\ t=0)]}{(s'-m^2)(s'-m^2+t)} \right\}, \quad (36)$$

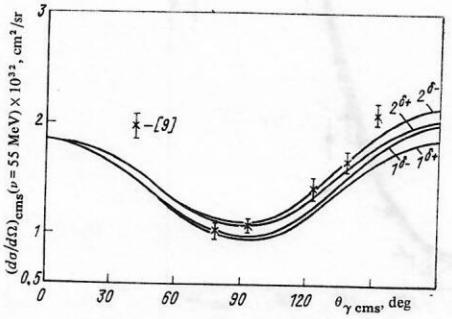

FIG. 13. Angular dependence of the differential cross section of γp scattering at 55 MeV: $1^{\delta-}$, $1^{\delta+}$, $2^{\delta-}$, $2^{\delta+}$ are the different variants of theoretical calculations.[73]

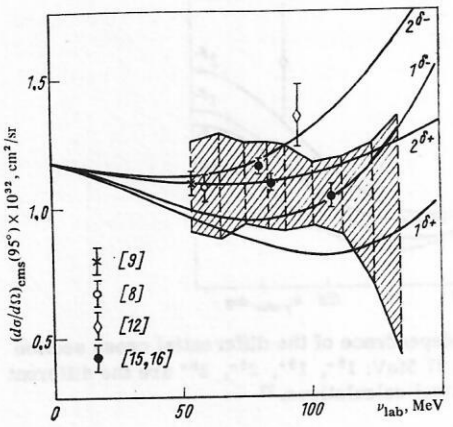

FIG. 14. Energy dependence of the differential cross section of γp scattering for the angle 95° in the center of mass system. The hatched region indicates the results of Ref. 3: $1^{\delta-}$, $1^{\delta+}$, $2^{\delta-}$, $2^{\delta+}$ are variants of theoretical calculations.[73] For the results of Refs. 15 and 16 the total errors of the experiments are given; for the results of Refs. 3, 9, 12, and 13 only the statistical errors.

where the $\bar{A}_i$'s mean that these amplitudes do not include terms expressed by means of the diagrams of fourth-order perturbation theory.

Comparison of experimental data with calculations made with fixed-t dispersion relations. Sign of the $\pi^0 \to 2\gamma$ decay amplitude

We now compare the experimental data with the predictions of theory in the energy range from 55 to 280 MeV. The results of calculations made on the basis of the dispersion relations (33) and (35) were found[76] to be close to the results of Refs. 73 and 75, in which the calculations were also made with fixed-t dispersion

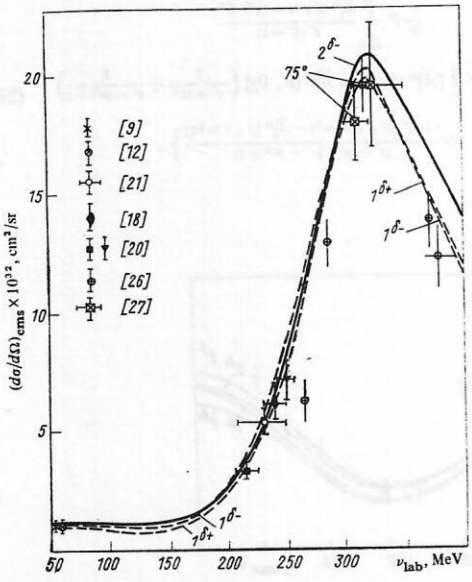

FIG. 15. Energy dependence of the differential cross section of γp scattering for the angle 70° in the center of mass system: $1^{\delta-}$, $1^{\delta+}$, $2^{\delta-}$, $2^{\delta+}$ are variants of theoretical calculations.[73]

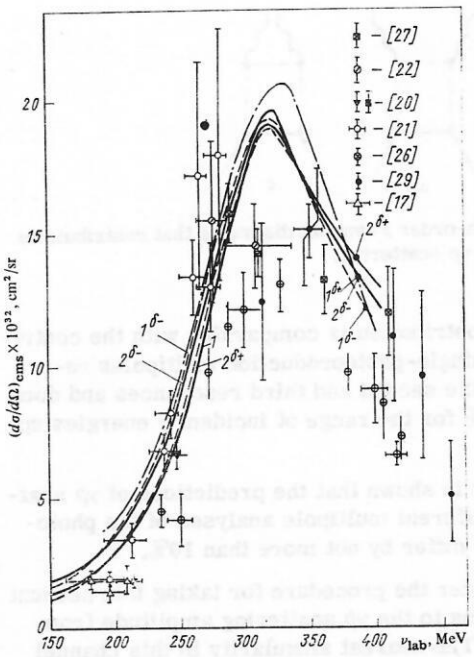

FIG. 16. Energy dependence of the differential cross section of γp scattering for the angle 90° in the center-of-mass system: $1^{\delta-}$, $1^{\delta+}$, $2^{\delta-}$, $2^{\delta+}$ are variants of theoretical calculations[73]; the dot-dash-dot curve shows the theoretical calculations of Ref. 69.

relations, but ones with a more complicated form than (33).

The experimental data[3, 9, 12, 13, 15, 16] and the theoretical

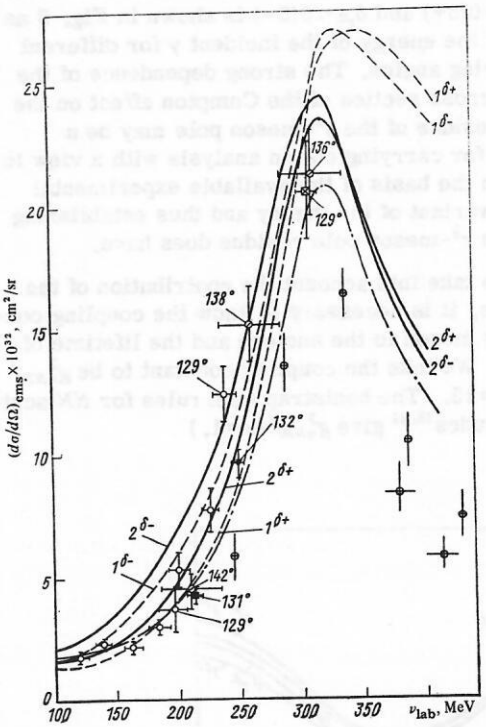

FIG. 17. Energy dependence of the differential cross section of γp scattering for the angle 139° in the center-of-mass system. The experimental points are denoted as in Figs. 15 and 16; $1^{\delta-}$, $1^{\delta+}$, $2^{\delta-}$, $2^{\delta+}$ are variants of theoretical calculations[73]; the dot-dash-dot curve shows the theoretical calculations of Ref. 69.

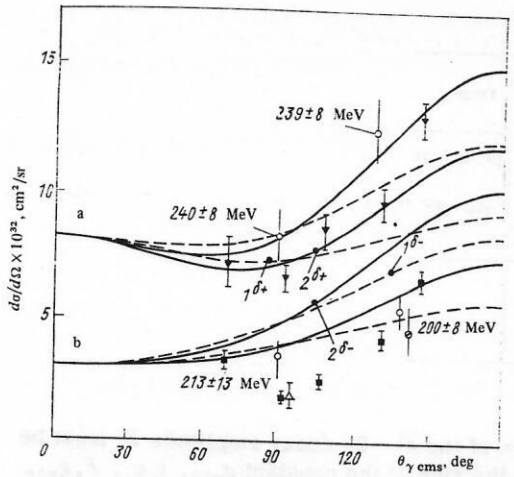

FIG. 18. Angular dependences of the differential cross section of γp scattering for different energies: a) $\nu = 249$ MeV; b) $\nu = 214$ MeV (see Ref. 20); $1^{\delta-}, 1^{\delta+}, 2^{\delta-}, 2^{\delta+}$ are variants of theoretical calculations[73]; the experimental points are denoted in the same way as in Figs. 15 and 16.

curves of Refs. 73–75 for the angular and energy dependences of the differential cross section of elastic scattering for the energy range below 150 MeV are shown in Figs. 11–14. The experimental and theoretical energy and angular dependences of the differential cross section for energies from 120 to 280 MeV are given in Figs. 15–18. It can be seen from Figs. 11–18 that the experimental data in the energy ranges 55–120 and 240–280 MeV agree satisfactorily with the theoretical calculations.

The detailed comparison[75,76,87,88] of the complete set of experimental data with the variants $1^{\delta\pm}$ and $2^{\delta\pm}$ of the theoretical calculations was based on the use of the χ^2 statistical test.

The experiments in the energy range 55–120 MeV are basically represented by the angular distributions[9,12,13] and the energy dependence.[3] In the energy range 240–280 MeV the experimental data are represented by the angular distribution of Ref. 20 at the mean γ energy 249 MeV and the energy dependence of the cross section[21] for the scattering angle 90° in the center-of-mass system. In the intermediate-energy range near the pion-photoproduction threshold one observes a fairly strong (in units of the accuracy of the measurements) deviation of the experimental data from all variants of the theoretical calculations. This is particularly marked in the angular distributions (see, for example, Fig. 18) for energies around $\nu = 214$ MeV. Therefore, the experimental points in the energy range 120–220 MeV (eight points altogether) are not included in the numerical analysis. The experimental data are compared with the theoretical studies in two ranges of γ energies: 55–120 and 240–280 MeV, in which the most complete experimental data are currently available.

Each of the four variants of theoretical calculations $1^{\delta\pm}$ and $2^{\delta\pm}$ made in Refs. 73–75 is analyzed to see if they are consistent with the experimental data. Each experimental investigation is first analyzed separately, and then the results of the analysis are combined in each energy range in accordance with the addition rules for the χ^2 distribution. For each of the variants of the theoretical calculations two quantities are determined: the value of the factor k corresponding to normalization of the results of each of the investigations separately to give best agreement with the chosen theoretical variant, and the value of the probability $P_f(\chi^2)$ (where f is the number of degrees of freedom). The theoretical calculations are also compared with the experiments for only the profile of the cross section as a function of the scattering angle or energy. The results of analyses obtained in the two ways agree well with one another.

Tables 5 and 6 give the result of this comparison: Table 5, of the analysis based on comparison of the theoretical variants[73,74] and the experiment as only regards the profile of the cross section as a function of the scattering angle[20] and the energy.[21] It can be seen from Table 5 that the experimental data of the individual investigation Ref. 20 at the 1% significance level rule out two of the four theoretical variants, namely, $1^{\delta+}$ and $1^{\delta-}$. At the 5% significance level, the variant $2^{\delta+}$ is also eliminated. The only variant that is consistent with the experimental data is $2^{\delta-}$. The experimental results of Ref. 21 reject only one variant at the 5% significance level.

The combined analysis of the experimental data of Refs. 20 and 21 does not in practice enable one to draw any new conclusions compared with those obtained from the analysis of Ref. 20. Table 6 gives the results of analysis for the γ-energy ranges 55–120 and 240–280 MeV. At low energies, the results of the three experimental investigations Refs. 9, 12, and 13 eliminate three of the four theoretical variants, namely, $1^{\delta+}$, $1^{\delta-}$, and $2^{\delta+}$, at the 5% significance level, as can be seen from Table 6. The results of the analysis made for each of the investigations separately showed that Ref. 12 does not eliminate any of the theoretical variants at the 5% significance level. The results of Ref. 13 eliminate only the variant $1^{\delta+}$, while the results of Ref. 9 eliminate two variants, namely, $1^{\delta+}$ and $2^{\delta+}$. The results of Refs. 3 and 10, in which the energy dependence of the cross section was investigated, do not eliminate any of the theoretical variants and therefore are not included in Table 6. It can also be seen from Table 6 that taken together the investigations, in the two γ-energy ranges 55–120 and 240–280 MeV already enable one to eliminate the variants $1^{\delta+}$, $1^{\delta-}$, and $2^{\delta+}$ at the 1% significance level.

TABLE V.

f	Variants of theoretical calculation								Rejection at 5% significance level	Literature
	$1^{\delta-}$		$1^{\delta+}$		$2^{\delta-}$		$2^{\delta+}$			
	k	p	k	p	k	p	k	p		
4	1.09	0.1%	0.92	0.01%	1.18	15%	0.99	3.8%	$1^{\delta+}$, $1^{\delta-}$,	[20]
6	0.93	10%	0.81	1.2%	0.94	31%	0.82	12%	$2^{\delta+}$, $1^{\delta+}$	[21]
10	0.1%		0.01%		17%		2.7		$1^{\delta+}$, $1^{\delta-}$, $2^{\delta+}$	[20, 21]

Note. The results of Ref. 20 are the angular dependence of the cross section at the mean γ energy 249 MeV; number of points used: $n = 5$. The results of Ref. 21 are the energy dependence of the cross section in the range 239–282 MeV; six points for the angle $\theta = 90°$ and one point for $\theta = 129°$.

TABLE VI.

Range of γ energies, MeV	f	Variants of theoretical calculations								Rejection at 5% significance level	Literature
		$1^{\delta-}$		$1^{\delta+}$		$2^{\delta-}$		$2^{\delta+}$			
		χ^2	p, %	χ^2	p, %	χ^2	p, %	χ^2	p, %		
55—120	11	23.39	1.6	31.33	0.1	17.90	8.0	20.67	3.6	$1^{\delta+}$, $1^{\delta-}$, $2^{\delta+}$	[9, 12, 13]
240—280	12	29.34	0.3	52.02	0.01	14.65	26.0	23.01	2.8	$1^{\delta+}$, $1^{\delta-}$, $2^{\delta+}$	[18, 21]
For both energy ranges and two groups of investigations	23	52.75	0.5	83.35	0.001	32.55	9.0	43.68	0.59	$1^{\delta+}$, $1^{\delta-}$, $2^{\delta+}$	

The results of the calculations in accordance with the dispersion relations (47) and (49), whose derivation[75,76] used weaker restrictions on the asymptotic behavior of the scattering amplitudes than the ones adopted in Refs. 73 and 74, were also compared with the experimental data. The results of the analysis are given in Table 7. To a considerable extent, they agree with the results given earlier. It can be seen from Table 7 that the experimental data obtained for the energy range 55—120 MeV eliminate two of the four theoretical variants ($1^{\delta\pm}$) at the 5% significance level. In the range 240—280 MeV the experimental data of the single investigation Ref. 20 eliminate three of the four variants ($1^{\delta\pm}$, $2^{\delta\pm}$). The only variant that does not contradict the experimental data is $2^{\delta-}$, as before. The results of a combined analysis of Refs. 9, 12, 13, 20, and 21 agree with the conclusions obtained from analysis of the results of Ref. 20 alone, as can be seen from Table 7.

Thus, the comparison of theory and experiment in the energy ranges below 120 and between 240 and 280 MeV show that at the 99% confidence level one can eliminate the theory in which the $\pi\pi$ interaction is taken into account solely by means of the diagrams of fourth-order perturbation theory (see Fig. 10) for any sign of the amplitude F_π and there remains only the theoretical variant in which, besides these diagrams, the annihilation channel is taken into account by means of the bootstrap model. This indicates, on the one hand, the need to make a more accurate allowance for the annihilation channel than is possible from calculations by means of the diagrams shown in Fig. 10, and, on the other, that the adopted model for the t channel is reasonable and that one obtains a satisfactory description of the interaction of particles by means of the bootstrap model.

At the 95% confidence level it has been established that the sign of the $\pi^0 \to 2\gamma$ decay amplitude F_π must be opposite to the sign of the constant $g_{\pi NN}$, i.e., $F_\pi g_{\pi NN} < 0$. This sign of the decay amplitude agrees with the sign predicted for this amplitude in Ref. 60, in which $\pi^0 \to 2\gamma$ decay through a nucleon-antinucleon pair[61] was treated by perturbation theory. The sign of F_π is different in different field-theory models.[89] The sign of the amplitude F_π, which was first found in Ref. 87, was used by Okubo[90] to choose between various known models of elementary particles. This sign of the amplitude F_π was later confirmed by Gilman[91] from the experimentally observed positive interference in π^0-meson photoproduction between the amplitude of the single-photon effect (the Primakoff effect) and the other photoproduction amplitudes.

It should be noted that in Ref. 92 a model-independent method of determining the sign of F_π is proposed on the basis of a measurement of the sign of the interference between the Primakoff effect and the nuclear part of the π^0-meson photoproduction. This method involves separating the nuclear background by means of finite-energy sum rules and an analysis of the angular distributions for different γ energies. Below, we shall consider the determination of the sign of F_π from low-energy γp scattering.

Kinematic singularities and determination of subtraction functions

In the expression (9), the coefficients of T_i have singularities of the form $\{t[st+(s-m^2)^2]\}^{-1}$. Since the total amplitude T_{fi} does not have kinematic singularities, these features impose relations between T_i for the forward and backward angles:

a) $t=0$:

$$T_1(s, 0) + T_3(s, 0) = 2T_5(s, 0); \tag{37}$$

TABLE VII.

f	Variants of theoretical calculations												Rejection at 5% significance level	Literature
	$1^{\delta-}$			$1^{\delta+}$			$2^{\delta-}$			$2^{\delta+}$				
	k	χ^2	p, %	k	χ^2	p, %	k	χ^2	p, %	k	χ^2	p, %		
12	—	21.95	3.7	—	22.90	2.8	—	15.16	22.0	—	17.52	13.2	$1^{\delta+}$, $1^{\delta-}$	[9, 12, 13]
7	0.99	6.39	49	1.10	9.12	24	1.00	4.91	67	1.13	8.22	31	—	[21]
5	0.78	11.6	4.1	0.92	16.14	0.6	0.78	9.42	9.4	0.91	11.2	4.9	$1^{\delta+}$, $1^{\delta-}$, $2^{\delta+}$	[20]
17	—	33.55	1.0	—	39.04	0.2	—	24.58	10.0	—	28.10	3.9	$1^{\delta+}$, $1^{\delta-}$, $2^{\delta+}$	[9, 12, 13, 20]
24	—	39.95	2.1	—	48.16	0.25	—	29.49	20.2	—	36.9	4.2	$1^{\delta+}$, $1^{\delta-}$, $2^{\delta+}$	[9, 12, 13, 20, 21]

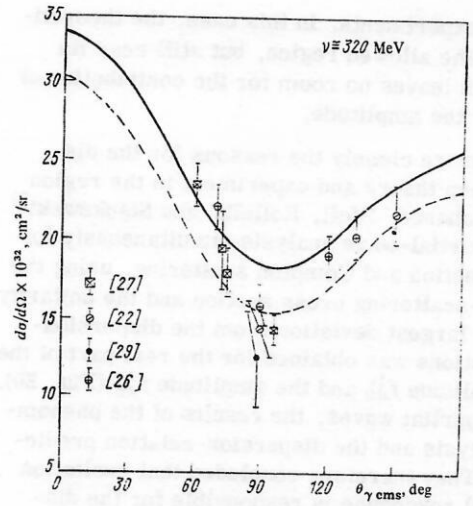

FIG. 19. Lower unitary limit for γp scattering at 320 MeV. The solid line corresponds to the analysis in Ref. 80 of the photoproduction data; the dashed curve shows the lowest possible values of the photoproduction multipoles.[79-81]

$$T_5(s, 0) = -(s-m^2)[T_2(s, 0) + T_4(s, 0)]/4m; \tag{38}$$

b) $t = -4\omega^2 = -(s-m^2)^2/s$:

$$T_1(s, t=-4\omega^2) - T_3(s, t=-4\omega^2) = 2mT_6(s, t=-4\omega^2): \tag{39}$$

$$T_6(s, t=-4\omega^2) = (s-m^2)[T_4(s, t=-4\omega^2) - T_2(s, t=-4\omega^2)]/[2(s+m^2)]. \tag{40}$$

Kinematic singularities can be avoided if one operates with Bardeen–Tung amplitudes.[93] However, in this case one cannot make a subtraction in the dispersion relation at the threshold (since some of the amplitudes have a second-order pole at the threshold) and, therefore, it is difficult to introduce low-energy theorems into the numerical calculations.

In the construction of dispersion relations for fixed scattering angle[45,69] and for fixed t the above connections between the amplitudes were not considered, and this may have led to the overestimated values of the calculated differential cross sections[78] for scattering through 180°.

Let us consider a dispersion relation for fixed t. In this case, the connections between the scattering amplitudes at $t=0$ are exactly satisfied, as is readily verified. And the relations between the backward-scattering amplitudes (39) and (40) can be used to determine some of the subtraction functions.

Let us write down the dispersion relation (31) for the amplitudes T_i with $i=1, 3, 5, 6$ and the dispersion relation (35) for T_j with $j=2, 4$. In accordance with (32), the subtraction function can be written in the form

$$\operatorname{Re} T_i(u_0, t) = r_i(1/(m^2-\bar{s}_0) + 1/(m^2-u_0)) + \operatorname{Re} T_i(u_0, t_0=0) + t\dot{\phi}(u_0, t). \tag{41}$$

Substituting (41) into (31) and going to the limit $u_0 \to m^2$, we obtain

$$\operatorname{Re} T_i(s, t) = r_i\left(\frac{1}{m^2-s} + \frac{1}{m^2-u}\right) + T_i(m^2, 0) - t\dot{\phi}_i(u=m^2, t) + \frac{u-m^2}{\pi} P \int_{(m+\mu)^2}^{\infty} ds' A_{1i}^{(s)}(s', t) \times \left\{\frac{1}{(s'-m^2)(s'-s)} - \frac{1}{(s'-m^2+t)(s'-s)}\right\}, \tag{42}$$

where $\phi_i(t)$ depends on the single variable t.

We require that the amplitude T_i expressed in terms of the dispersion relations (42) and (35) satisfy the conditions (39) and (40) for t and s related by the condition $t = -(s-m^2)^2/s$. After simple transformations, we obtain an expression for the subtraction functions $\phi_i(m^2)$ in terms of integrals in the s channel:

$$\dot{\phi}_1(m^2, t) - \dot{\phi}_3(m^2, t) = \frac{1}{\pi} P \int_{(m+\mu)^2}^{\infty} \frac{dx}{(x-s_1)(x-m^4/s_1)} \times \left\{\frac{m^2(2xs_1 - s_1^2 - m^4)}{s_1(x-m^2)(x-m^2+t)}[A_1^{(s)}(x, t) - A_3^{(s)}(x, t)] - 2m[A_4^{(s)}(x, t) - A_2^{(s)}(x, t)]\right\}; \tag{43}$$

$$\dot{\phi}_6(m^2, t) = \frac{1}{\pi} P \int_{(m+\mu)^2}^{\infty} \frac{dx}{(x-s_1)(x-m^4/s_1)} \times \left\{\frac{2m^2(2xs_1 - s_1^2 - m^4)}{s_1(x-m^2)(x-m^2-t)} A_6^{(s)}(x, t) - [A_4^{(s)}(x, t) - A_2^{(s)}(x, t)]\right\}, \tag{44}$$

where

$$s_1 = m^2 - t/2 + \sqrt{t(t-4m^2)}/2.$$

Thus, in the dispersion relation two of the four subtraction functions are determined by (43) and (44). The functions $\phi_1(t) + \phi_3(t)$ and $\phi_5(t)$, as before,[75,76] are given by

$$\dot{\phi}_1(t) + \dot{\phi}_3(t) = \frac{1}{\pi} \int_{4\mu^2}^{\infty} \frac{A_1^{(t)}(t', u=m^2) + A_3^{(t)}(t', u=m^2)}{t'(t'-t)} dt' - \frac{1}{\pi} P \int_{(m+\mu)^2}^{\infty} \frac{A_1^{(s)}(s', u=m^2) + A_3^{(s)}(s', u=m^2)}{(s'-m^2)(s'-m^2+t)} ds'; \tag{45}$$

$$\dot{\phi}_5(t) = \frac{\delta_\pi}{\mu_{\pi^0}^2(\mu_{\pi^0}^2 - t)} + \frac{1}{\pi} P \int_{4\mu^2}^{\infty} \frac{A_5^{(t)}(t', u=m^2)}{t'(t'-t)} dt' - \frac{1}{\pi} P \int_{(m+\mu)^2}^{\infty} \frac{A_5^{(s)}(s', u=m^2) ds'}{(s'-m^2)(s'-m^2-t)}. \tag{46}$$

The dispersion relations (42) and (35) with the subtraction functions we have obtained satisfy the kinematic relations (37)–(40). However, numerical calculations have not yet been made with these dispersion relations.

Compton scattering in the region of the $P_{33}(1236)$ resonance

Let us consider scattering of γ's on protons in the region of the $P_{33}(1236)$ resonance. Discrepancies between dispersion-relation predictions and experiments near this resonance were noted already in the early investigations of γp scattering, and the later experimental data have only aggravated the discrepancy. It was assumed that this is due to the poor determination of the real part of the amplitude because of inaccurate allowance for the total contribution of the small photoproduction amplitudes and incomplete treatment of the t-channel contribution.

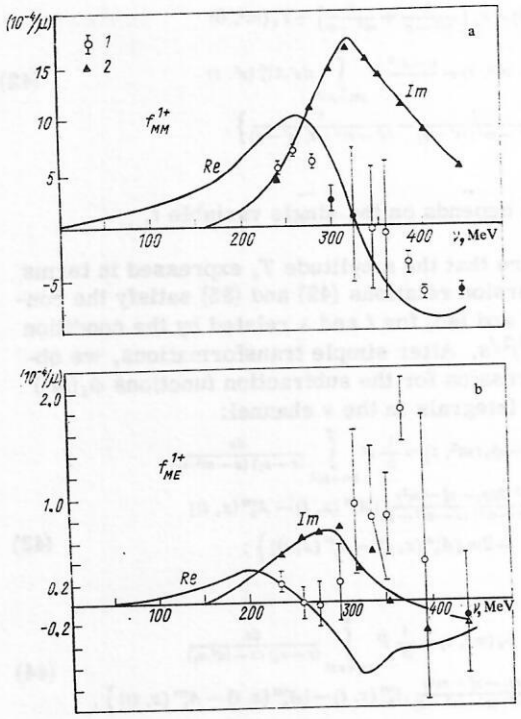

FIG. 20. Real and imaginary parts of partial waves. a) f_{MM}^{1+}; b) f_{ME}^{1+};1) fitting of real parts of partial waves; 2) fitting of imaginary parts of partial waves; the continuous curves are the results of calculations using dispersion relations.[78]

Pfeil, Rollnik, and Stankowski[78] calculated the differential cross section of γp scattering under the assumption that the real part of the amplitude is zero. Since the real and the imaginary parts of the amplitudes occur independently in the differential cross section (10), they obtained in this manner the minimal theoretical value of the γp differential-scattering cross section. In this case, there is no need to use dispersion relations, and the imaginary part of the amplitude can be expressed by means of the unitarity condition in terms of the pion-photoproduction amplitudes. The photoproduction data given in Refs. 79–81 were used in Ref. 78.

The differential cross sections obtained in this manner lie below the experimental values at energies below 300 MeV and above 380 MeV. In the range between 300 and 380 MeV, the theoretical predictions are almost saturated by the experimental data.

At the resonance energy (320 MeV) for the angle $\theta = 90°$ the theoretical curve (Fig. 19, continuous curve) passes above the experimental data, and the discrepancy is at least two standard deviations.

This discrepancy is due to the exceptionally large contribution of the resonance-photoproduction multipole M_{1+}. The most important reduction of the differential cross section is due to the interference of E_{1+} and M_{1-} with M_{1+}. Therefore, better agreement with the experiment can be achieved only by reducing the amplitude M_{1+} (and E_{0+}) and increasing E_{1+} (and M_{1-}). In Fig. 19, the dashed curve gives the results obtained with the smallest M_{1+} (and E_{0+}) and largest E_{1+} (and M_{1-}) values allowed by the experiments. In this case, the theoretical curve is in the allowed region, but still near its boundary, which leaves no room for the contribution of the real part of the amplitude.

To examine more closely the reasons for the discrepancy between theory and experiment in the region of the first resonance, Pfeil, Rollnik, and Stankowski[78] carried out a partial-wave analysis simultaneously for pion photoproduction and Compton scattering, using the γp differential-scattering cross section and the unitarity condition. The largest deviation from the dispersion-relation predictions was obtained for the real part of the resonance amplitude f_{MM}^{1+} and the amplitude f_{ME}^{1+} (Fig. 20). For the other partial waves, the results of the phenomenological analysis and the dispersion-relation predictions agreed. They therefore concluded that excitation of the $P_{33}(1236)$ resonance is responsible for the discrepancy, and not the summed effect of small amplitudes. They concluded that it is either necessary to reexamine the importance of the $P_{33}(1236)$ resonance in γp scattering or to change the experimental data appreciably.

4. SUM RULES

Gerasimov–Drell–Hearn sum rules

The amplitude of forward γp scattering has the form

$$\bar{u}_2 T_{f_i u_1} = (\mathbf{e}_2 \mathbf{e}_1) f_1(\nu) + i(\sigma [\mathbf{e}_2 \mathbf{e}_1]) f_2(\nu), \tag{47}$$

where f_1 and f_2 are related to the amplitudes R_i in (13) by

$$f_1 = R_1(\nu) + R_2(\nu);$$
$$f_2 = R_3(\nu) + R_4(\nu) + 2[R_5(\nu) + R_6(\nu)].$$

Let us consider the amplitude $f_2(\nu)$. It is antisymmetric under the replacement of ν by $-\nu$. Suppose that for this amplitude we can write down unsubtracted dispersion relations in ν. Constructing these relations at the point $\nu = 0$ and using the low-energy limit for $\mathrm{Re} f_2(\nu)/\nu$ as $\nu \to 0$, we obtain

$$-\frac{e^2 \lambda_p^2}{2m^2} = \frac{2}{\pi} \int_{\nu_0}^{\infty} \frac{d\nu}{\nu^2} \mathrm{Im}\, f_2(\nu).$$

Expressing the imaginary part of the amplitude $f_2(\nu)$ in terms of the difference of the total cross sections of photoabsorption of photons whose spins are parallel (σ_p) and antiparallel (σ_a) to the proton spin, we obtain the following final form of the sum rules:

$$\frac{\pi e^2 \lambda_p^2}{2m^2} = \int_{\nu_0}^{\infty} \frac{d\nu}{\nu} [\sigma_p(\nu) - \sigma_a(\nu)]. \tag{48}$$

These sum rules were originally constructed by Gerasimov,[95] and then by Drell and Hearn.[96] The sum rules (48) are saturated by low-lying resonances. These sum rules were obtained under the assumption that unsubtracted dispersion relations can be written down for the amplitude $f_2(\nu)$. Such an assumption is valid if the difference of the cross sections σ_p and σ_a does not contain an energy-independent contribution. Since the difference $\sigma_p - \sigma_a$ is characterized by negative τP, the pomeron pole (τP positive) does not contribute to this difference. The pomeron–pomeron cuts can have negative τP and, therefore, contribute to $\sigma_p - \sigma_a$. If this

contribution tends to a constant, one needs a subtracted dispersion relation, and the sum rules (48) will no longer hold.

Thus, the direct measurement of $\sigma_p(\nu)$ and $\sigma_a(\nu)$, especially for large ν, enables one to verify these sum rules and obtain additional information about the Regge trajectories with τP negative. A direct experimental verification of this kind has not yet been made.

Sum rules for the $\pi^0 \to 2\gamma$, $\eta \to 2\gamma$, $X^0 \to 2\gamma$ decay amplitudes

Let us consider the sum rules[97] for the $\pi^0 \to 2\gamma$, $\eta \to 2\gamma$, and $X^0 \to 2\gamma$ decay amplitudes. These sum rules enable one to obtain additional information about the π^0, η, and X^0 mesons. Suppose that the amplitude T_5 of γN scattering to which these mesons contribute tends to a constant limit with respect to s as $s \to \infty$ for fixed $t \leq 0$. Then for T_5 we can write down the dispersion relations

$$T_5(s,t) = r_5\left(\frac{1}{m^2-s}+\frac{1}{m^2-u}\right) + \frac{1}{\pi}\int\limits_{(m+\mu)^2}^{\infty} ds' A_5^{(s)}(s',t)\left[\frac{1}{s'-s}+\frac{1}{s'-u}\right] + \Lambda(t), \tag{49}$$

where the function $\Lambda(t)$ depends only on t. The possibility of writing down an unsubtracted integral of $A_5(s,t)$ follows from Regge-pole theory.

For T_5 we write down the Mandelstam representation:

$$T_5(s,u,t) = \frac{1}{\pi^2}\int\limits_{m^2}^{\infty}\frac{ds'}{s'-s}\int\limits_0^{\infty}\frac{dt'}{t'-t}\rho_{13}(s',t') + \frac{1}{\pi^2}\int\limits_{m^2}^{\infty}\frac{du'}{u'-u}\int\limits_0^{\infty}\frac{dt'}{t'-t}\rho_{23}(u',t') + \frac{1}{\pi^2}\int\limits_{m^2}^{\infty}\frac{ds'}{s'-s}\int\limits_{m^2}^{\infty}\frac{du'}{u'-u}\rho_{12}(s',u') + \frac{1}{\pi}\int\limits_{m^2}^{\infty}\frac{a_1(s')\,ds'}{s'-s} + \frac{1}{\pi}\int\limits_{m^2}^{\infty}\frac{a_2(u')\,du'}{u'-u} + \frac{1}{\pi}\int\limits_0^{\infty}\frac{a_3(t')\,dt'}{t'-t}. \tag{50}$$

The last three terms in (50) are quasilocal terms that depend only on s, u, and t, respectively. We go over from the double dispersion relations to one-dimensional ones at fixed t:

$$T_5(s,t) = r_5\left(\frac{1}{m^2-s}+\frac{1}{m^2-u}\right) + \frac{1}{\pi}\int\limits_{(m+\mu)^2}^{\infty} ds' A_5^{(s)}(s',t)\left[\frac{1}{s'-s}+\frac{1}{s'-u}\right] + \frac{1}{\pi}\int\limits_0^{\infty}\frac{a_3(t')\,dt}{t'-t}. \tag{51}$$

It follows from comparison of (49) and (51) that

$$\Lambda(t) = \lim T_5(s,t) = \frac{1}{\pi}\int\limits_0^{\infty}\frac{a_3(t')\,dt'}{t'-t}. \tag{52}$$

Setting $s=m^2$ and $t=0$ in (49) and taking into account the low-energy limit (34) for the amplitude $T_5(s=m^2, t=0)$, we obtain the sum rules[97]

$$T_5(s=m^2,t=0) = \frac{e^2}{2m}\left[(2\lambda_p+\lambda_p^2)\frac{1+\tau_3}{2}+\lambda_n^2\frac{1-\tau_3}{2}\right] = \Lambda(t=0) + \frac{2}{\pi}\int\limits_{(m+\mu)^2}^{\infty}\frac{A_5^{(s)}(s',t=0)}{s'-m^2}ds'. \tag{53}$$

Let us consider the isovector part of the amplitude T_5. If the π^0 meson is a moving Regge pole, its contribution to $\Lambda^{(V)}(t=0)$ is zero, but if it is an "elementary" particle, its contribution to $\Lambda^{(V)}(t=0)$ is nonzero. Suppose that the π^0 meson is not a Regge pole and that it makes the main contribution to $\Lambda^{(V)}(t=0)$; we then obtain sum rules for the $\pi^0 \to 2\gamma$ decay amplitude[97]:

$$\frac{g_{\pi NN}F_\pi}{2} = \frac{e^2}{4m}[2\lambda_p+\lambda_p^2-\lambda_n^2] - \frac{2}{\pi}\int\limits_{(m+\mu)^2}^{\infty}\frac{A_5^{(s,V)}(s',t=0)}{s'-m^2}ds', \tag{54}$$

where F_π, the $\pi^0 \to 2\gamma$ decay amplitude, has the form (20).

Similar sum rules were obtained by Pagels,[98] though later, under the assumption that $T_5(s,t=0) \underset{s\to\infty}{\to} 0$ and the π^0 meson is a Regge pole and appears in the expression (49) because of the representation $A_5^{(s,V)}$ as the sum $A_5^{(s,V)} = A_5^{(s,V)} + \mathcal{R}_5$, where the Regge part $\mathcal{R}_5$ is due solely to the high-energy contribution to $A_5^{(s,V)}$.

The assumption made in Ref. 97 in the derivation of (54) that the π^0 meson is not a Regge pole can be verified by calculating with sufficient accuracy the integral of $A^{(s,V)}(s,0)$ in the expression (54).

To calculate $A_5^{(s,V)}(s,0)$, we restrict ourselves to the contribution of single-pion photoproduction. In the photoproduction amplitudes we shall retain partial waves with $J \leq \frac{5}{2}$. We take the values of these partial waves from Ref. 82. As a result, we obtain

$$g_{\pi NN}F_\pi/2 = (0.072+0.023)/m = 0.095/m. \tag{55}$$

As can be seen from (55), the contribution of the integral is comparatively small and leads to an increase of the amplitude $g_{\pi NN}F_\pi$. The value found for $g_{\pi NN}F_\pi/2$ corresponds to the π^0-meson lifetime $\tau_{\pi^0} = 2.4\times10^{-16}$ sec.

It follows from (55) that F_π has the same sign as $g_{\pi NN}$. This is in contradiction with the sign of F_π found experimentally from γp scattering.[75,76,87,88]

The same sign of F_π as is obtained by means of the present sum rules[97] also follows from Pagels's paper, and also from the superconvergent sum rules[1)] with respect to u and t for fixed $s=0$ for the γN scattering amplitudes.[99] To reconcile these results with the experimental data,[87] it is necessary to introduce into (54) an additional term to ensure the correct sign of F_π. It is hardly probable that the required compensation can take place through more accurate allowance for the integral terms, since such compensation requires that the integral of $A_5^{(s,V)}$ in (54) be large and positive. But then, in accordance with the dispersion relation (33) for the amplitude T_5, this would increase T_5, and therefore increase the differential cross section of γp scattering, which would only aggravate the discrepancy between theory and experiment in the energy range 180–220 MeV and around 320 MeV.

This additional term may appear as the contribution of the quasilocal term $\Lambda_0^{(V)}$ to the left-hand side of (54). At the same time, it follows from the requirement of the correct sign and amplitude of F_π that[97]

$$\Lambda_0^{(V)}(t=0) \equiv \Lambda_0 \sim 2\,|\,g_{\pi NN}F_\pi/2\,|.$$

[1)] In Ref. 90, Okubo makes the erroneous assertion that the sum rules of Refs. 98 and 99 indicate that F_π has a sign opposite to $g_{\pi NN}(g_{\pi NN}F_\pi < 0)$, i.e., in agreement with the experimental value.[87]

Since $\Lambda_0^{(V)}(t)$ occurs in the amplitude $T_5^{(V)}$ and does not depend on s, the state in the annihilation channel that contributes to $\Lambda_0^{(V)}$ has the following quantum numbers: $I=1$, $G=-1$, $P=-1$, $C=+1$, $J=0$, i.e., the quantum numbers of the π^0 meson.

We parametrize the function $\Lambda_0^{(V)}(t)$ (for $t \leq 0$) in the form

$$\Lambda_0^{(V)}(t) = \Lambda_0 m_e^2/(m_e^2 - t). \tag{56}$$

This term must appear in the dispersion relation (33) from the integral of $A_5^{(t)}(t, m^2)$, and with allowance for (56) it will have the form

$$\Lambda_0^{(V)}(t) - \Lambda_0^{(V)}(0) = \Lambda_0 t/(m_e^2 - t), \tag{57}$$

leading to a reduction of the differential cross section of γp scattering through an angle $\theta \neq 0$ at incident γ-ray $\nu < 300$ MeV. In principle, the effective mass m_0 may be small if $\Lambda_5^{(V)}$ is due, for example, to the contribution of an "antibound" state of a system of three pions. However, m_e cannot be too small ($m_e \sim \mu_{\pi^0}$), since then the total effect of the π^0-meson pole and the quasilocal term in the differential cross section of γp scattering would be the same as if one allowed for only the contribution of the π^0-meson pole with a sign that reduces the differential cross section ($g_{\pi NN} F_\pi < 0$), which would contradict the existing experimental data.[87]

The quasilocal term (57) can make an important contribution to the angular distribution of γp scattering at high energies. From the point of view of the J plane, this quasilocal term can be a fixed pole or a Kronecker singularity with the quantum numbers of the π^0 meson.

Let us now consider the sum rules (53) for the isoscalar part of the amplitude T_5. We shall assume that the η and X^0 mesons are "elementary" particles and make the main contribution to $\Lambda^{(S)}(0)$. Then[87]

$$\frac{g_{\eta NN} F_\eta}{2} + \frac{g_{X^0 NN} F_{X^0}}{2} = \frac{e^2}{4m}[2\lambda_p + \lambda_p^2 + \lambda_n^2] - \frac{2}{\pi}\int_{(m+\mu)^2}^{\infty} \frac{A_5^{(s,S)}(s', t=0)}{s'-m^2}\, ds', \tag{58}$$

where $g_{\eta NN}$ and $g_{X^0 N\Lambda}$ are the coupling constants of the interaction between the η and X^0 mesons and nucleons;

$$F_\eta^2 = 64\pi\Gamma_{\eta\to 2\gamma}/\mu_\eta^3; \quad F_{X^0}^2 = 64\pi\Gamma_{X^0\to 2\gamma}/\mu_{X^0}^3.$$

The assumption made above about the nature of the η and X^0 mesons can be verified by calculating with sufficient accuracy the integral of $A_5^{(s,S)}(s, t=0)$ if one knows the experimental values of the constants for the decay of the η and X^0 mesons into two γ's and the coupling constants of the interaction between these mesons and nucleons.

To calculate the integral of $A_5^{(s,S)}(s, 0)$, we again restrict ourselves to allowing for the contribution of the amplitudes for the photoproduction of single mesons on a nucleon and we use Walker's phenomenological analysis of photoproduction.[82] As a result, the relation (58) takes the form

$$g_{\eta NN} F_\eta/2 + g_{X^0 NN} F_{X^0}\, 2 = (0.239 - 0.428)/m = -0.189/m.$$

Let us estimate the amplitude $g_{X^0 NN} F_{X^0}$. To this end, we take for $g_{\eta NN}$ the value obtained from analysis of the bootstrap sum rules[83,84] for the amplitudes of baryon–baryon scattering, i.e., $g_{\eta NN}^2/4\pi = 1.05$. In accordance with Ref. 86, we take the $\eta \to 2\gamma$ decay width equal to 0.37 keV. The sign of F_η relative to $g_{\eta NN}$ is unknown, and we therefore consider two possibilities:

1) $g_{\eta NN} F_\eta > 0$; then $g_{X^0 NN} F_{X^0} = -0.51/m$;

2) $g_{\eta NN} F_\eta < 0$; then $g_{X^0 NN} F_{X^0} = -0.25/m$.

If we take the coupling constant to be $g_{X^0 NN}^2/4\pi \approx 1$, then in the first case we have $\Gamma_{X^0\to 2\gamma} \approx 100$ keV and in the second $\Gamma_{X^0\to 2\gamma} \approx 25$ keV.

5. γp SCATTERING AT LOW ENERGIES

Determination of the generalized polarizability of the proton from γp scattering

When low-energy γ's are scattered on the proton, the scattering amplitude can be represented as an expansion in the γ energy ν. Using relativistic and gauge invariance, Low[100] and Gell-Mann and Goldberger[101] found that the coefficients of the zeroth and first powers of ν can be expressed solely in terms of the constant of the electric charge e and the anomalous magnetic moment of the proton. The amplitude of Compton scattering in the second order in ν is determined by two structure constants as well as by e and λ_p. These constants are called[104] the generalized electric ($\bar{\alpha}$) and magnetic ($\bar{\beta}$) polarizabilities of the proton. Klein[102] was the first to point out the connection between the quadratic terms in the spin-independent amplitudes and the electric and magnetic polarizabilities of the proton. Baldin[103] obtained an explicit expression for the electric polarizability $\bar{\alpha}$, this agreeing with the generally adopted expression in nonrelativistic theory, and he estimated the value.

As was shown by Petrun'kin,[104] the amplitude of γp scattering in the expansion in ν to terms ν^2 can be represented in the following form (in the laboratory system):

$$\begin{aligned}\bar{u}(p_2) T_{fi} u(p_1) = &\left[-\frac{e^2}{m} + 4\pi\bar{\alpha}\nu_1\nu_2\right](\mathbf{e}_2\mathbf{e}_1) \\ &+ \nu_1\nu_2\left[4\pi\bar{\beta} - \frac{e^2}{4m^3}(1+\lambda_p)^2\cos\theta_\Lambda\right](\mathbf{s}_2\mathbf{s}_1) \\ &+ i(\nu_1+\nu_2)\frac{e^2(1+2\lambda_p)}{4m^2}\left(\sigma[\mathbf{e}_2\mathbf{e}_1]\right) + i(\nu_1+\nu_2)\frac{e}{4m^2} \\ &\times (1+\lambda_p)^2(\sigma[\mathbf{s}_2\mathbf{s}_1]) + i\frac{e}{2m^2}(1+\lambda_p)^2 \\ &\times [\nu_2(\sigma\mathbf{s}_2)(\varkappa_2\mathbf{e}_1) - \nu_1(\sigma\mathbf{s}_1)(\varkappa_1\mathbf{e}_2)],\end{aligned} \tag{59}$$

where

$$\left.\begin{aligned}&\bar{\alpha} = \alpha + 1/3 \langle r_e^2 \rangle + \lambda_p e^2/2m^3 + 3e^2/4m^3 + \Delta\alpha; \\ &\bar{\beta} = \beta + \Delta\beta.\end{aligned}\right\} \tag{60}$$

In the expressions (60), $\Delta\alpha$ and $\Delta\beta$ are unknown corrections to the polarizabilities α and β; $\langle r_e^2 \rangle$ is the mean square radius of the proton charge distribution. As can be seen from (59), $\bar{\alpha}$ and $\bar{\beta}$ contribute to the coefficients of ν^2 in the amplitudes R_1 and R_2 in (13):

$$\left.\begin{aligned}&\bar{R}_1 = \nu_1\nu_2 4\pi\bar{\alpha}; \\ &\bar{R}_2 = \nu_1\nu_2[4\pi\bar{\beta} - (e^2/4m^3)(1+\lambda_p)^2\cos\theta_\Lambda].\end{aligned}\right\} \tag{61}$$

Barashenkov *et al.*[105,106] obtained an expansion of the γp scattering amplitude to terms ν^3. No new constants appeared in the expansion.

The differential cross section of Compton scattering on the proton can in accordance with Refs. 104–106 be represented as an expansion in ν of the form

$$(d\sigma/d\Omega)_0 = (d\sigma/d\Omega)_p - (e^2/4\pi m)^2 \nu^2 [\bar{\alpha}(1+z^2) + 2\bar{\beta}z] \times (1 - 3\nu(1-z)/m) + 0(\nu^4), \quad (62)$$

where $z = \cos\theta_\Lambda$. The first term in (62) is the scattering cross section of a γ on a structureless particle with spin $\frac{1}{2}$ (see Ref. 35):

$$(d\sigma/d\Omega)_p = (e^2/4\pi m)^2 \{[1 - 2\nu/m(1-z) + 3(\nu/m)^2(1-z)^2 - 4(\nu/m)^3(1-z)^3](1+z) + (\nu/m)^2[(1-z)^2 + f(\theta)]\}/2, \quad (63)$$

where

$$f(\theta) = a_0 + a_1 z + a_2 z^2; \quad a_0 = 2\lambda_p + 9\lambda_p^2/2 + 3\lambda_p^3 + 3\lambda_p^4/4;$$
$$a_1 = -4\lambda_p - 5\lambda_p^2 - 2\lambda_p^3; \quad a_2 = 2\lambda_p + \lambda_p^2/2 - \lambda_p^3 - \lambda_p^4/4.$$

For the sum $\bar{\alpha} + \bar{\beta}$ of the polarizabilities one can construct sum rules that relate $\bar{\alpha} + \bar{\beta}$ to the integral of the total photoabsorption cross section. To this end, we write down the Kramers–Kronig dispersion relation[48,49] for the sum of the amplitudes $R_1 + R_2$ at $\theta = 0°$. We obtain[103,107]

$$\bar{\alpha} + \bar{\beta} = \frac{1}{2\pi^2} \int_{\nu_0}^{\infty} \frac{\sigma(\nu)}{\nu^2} d\nu. \quad (64)$$

If we substitute the experimental values of $\sigma(\nu)$ right up to the energy 30 GeV (see Refs. 108 and 109) into (64) and use the usual Regge extrapolation to higher energies, we obtain[116,117]

$$\bar{\alpha} + \bar{\beta} = (14.1 \pm 0.3)\, 10^{-43}\ \text{cm}^3. \quad (65)$$

The first experimental indication that the polarizability of the proton influences the differential cross section of elastic scattering of γ's on protons was obtained in Ref. 13 in 1956. Then, in Ref. 9, Gol'danskiĭ *et al.* were the first to determine the value of the proton's coefficients of electric and magnetic polarizability:

$$\bar{\alpha} = (9 \pm 2) \times 10^{-43}\ \text{cm}^3;$$
$$\bar{\beta} = (2 \pm 2) \times 10^{-43}\ \text{cm}^3, \quad (66)$$

where the errors correspond to the statistical errors of the measured yields. These results were obtained with the use of the expression (62) (restricted to quadratic terms in ν) for analysis of the experimental data on γp scattering at energy $\nu = 55$ MeV, and (64) was also used. In this relation, $\sigma(\nu)$ was expressed in terms of the experimental data for the cross section of single-pion photoproduction in the range of incident γ energies up to 1 GeV, which gave $\bar{\alpha} + \bar{\beta} = 11 \times 10^{-43}\ \text{cm}^3$.

Baranov *et al.*,[15,16] using new and more accurate experimental data for the energies from 80 to 110 MeV for scattering angles 90 and 150° in the analysis by means of Eq. (62), obtained the following values of $\bar{\alpha}$ and $\bar{\beta}$:

$$\left.\begin{aligned} \bar{\alpha} &= (10.7 \pm 1.1) \times 10^{-43}\ \text{cm}^3; \\ \bar{\beta} &= (-0.7 \pm 1.6) \times 10^{-43}\ \text{cm}^3 \end{aligned}\right\} \quad (67)$$

and accordingly

$$\bar{\alpha} + \bar{\beta} = (10.0 \pm 2.3)\ 10^{-43}\ \text{cm}. \quad (68)$$

The possible errors of the theoretical expression (62) associated with neglect of the terms of fourth and higher powers in the frequency were not included in (66)–(68).

From comparison of (68) with the prediction of the sum rules (64) it can be seen that the value of the sum $\bar{\alpha} + \bar{\beta}$ obtained from the γp-scattering experiments agrees with (65) to within two standard deviations.

Allowance for the π^0-meson pole in the determination of the proton polarizability

Sign of the $\pi^0 \to 2\gamma$ decay amplitude. As was shown above, to determine the coefficients of the generalized proton polarizability from the experimental data on γp scattering at low energies, the expression (63) for the differential cross section of γp scattering, obtained from the general requirements of field theory as a series in powers of the energy ν of the incident γ with allowance for terms up to ν^3 inclusively, was used in Refs. 9, 15, and 16. It was also assumed that the contribution of the ignored terms is small in the investigated range of energies.

However, from analysis of γp scattering by means of dispersion relations it follows that the contribution of the π^0-meson pole, which enters the differential cross section with terms beginning with ν^4, is not small (see, for example, Fig. 13) and for $\nu = 100$ MeV and $\theta = 150°$ is about 10%. Therefore, allowance for the π^0-meson pole may be important when one deduces $\bar{\alpha}$ and $\bar{\beta}$ from γp scattering data.

It is easy to show that the radius of convergence of the expansion of the π^0-meson pole with respect to ν for scattering angle 90° is $\mu_{\pi^0}/\sqrt{2}$, while it is $\mu_{\pi^0}/2$ for scattering angle 180°. Thus, in this range of energies this pole must be taken into account completely without an expansion in ν.

The differential cross section of γp scattering with allowance for the π^0-meson pole has the form (in the laboratory system)[110]

$$d\sigma/d\Omega = \left(\frac{d\sigma}{d\Omega}\right)_0 + (2/m^2)(\nu/\mu_{\pi^0})^2 \times (1-z)/[1 + \nu(1-z)/m]^3 B_\pi (B_\pi + A) + 0(\nu^4), \quad (69)$$

where

$$B_\pi = (\mu_{\pi^0}/2\pi)\, g_{\pi NN} F_\pi t/(\mu^2 - t);$$
$$A = (e^2/4\pi)(\mu/2m)\{(2 + \lambda_p)^2 - 1 - (1 + \lambda_p)(1-z) \times (1 + 2\nu/m)/[1 + \nu(1-z)m]\};$$
$$t = -2\nu^2(1-z)/[1 + \nu(1-z)/m].$$

The expression for $(d\sigma/d\Omega)_0$ is determined by (62). The π^0-meson pole occurs in the amplitude T_5 in (9). As can be seen from (11), this pole occurs in the cross section in the form of a quadratic term and interference with other contributions in T_5. In (69), allowance is made for the interference of the π^0-meson pole with only the Born term. The dispersion integrals of the amplitude T_5 contribute to the cross section beginning with ν^4 (for interference with the Born term). These integrals were calculated by means of the dispersion relation (33). For energy $\nu = 100$ MeV their contribution to the amplitude T_5 is about 50% of the contribution of the π^0-meson pole (with the same sign as A). In what follows, we shall assume that the contributions of the remaining ignored terms do not exceed the retained term and that the error introduced by the ignored terms in (69) in the range of energies around 100 MeV is about ± 50% of the contribution of the π^0-meson pole. For a more accurate calculation of the indeterminacy in-

TABLE VIII.

Coefficient	$g_{\pi NN}F_\pi<0$	$g_{\pi NN}F_\pi=0$	$g_{\pi NN}F_\pi>0$	Δ
$\bar{\alpha}\cdot10^{43}$, cm^3	13.9	10.7	8.0	±2.1
$P_{90°}$, %	9	25	−50	—
$(\bar{\alpha}-\bar{\beta})\times10^{43}$, cm^3	19.9	11.4	4.4	±4.4
$P_{150°}$, %	12	1.3	0.7	—

troduced into $\bar{\alpha}$ and $\bar{\beta}$ by the omitted terms it would be necessary to calculate the expression (69) by means of dispersion relations and the value of $d\sigma/d\Omega$ without expansion in ν and find their difference.

In Ref. 110, Eq. (69) was used to analyze the experimental data of Refs. 15 and 16 in the energy range 80–110 MeV separately for $\theta=90$ and 150°. From the analysis for $\theta=90°$ the value of $\bar{\alpha}$ was found, and the analysis for $\theta=150°$ made it possible to determine directly the difference $\bar{\alpha}-\bar{\beta}$. The results are presented in Table 8 for different ways of allowing for the π^0-meson pole. The $\pi^0\to2\gamma$ decay width was taken from Ref. 113 to be equal to $\Gamma_{\pi^0\to2\gamma}=7.7\pm0.9$ eV.

Table 8 gives the probabilities $P_+(\chi^2)$ for three different ways of treating the π^0-meson pole and also the total experimental and (assumed) theoretical errors in $\bar{\alpha}$ and $\bar{\alpha}-\bar{\beta}$.

It can be seen from Table 8 that the polarizability difference $\bar{\alpha}-\bar{\beta}$ is particularly sensitive to the contribution of the π^0-meson pole. Analysis of the data for the angle $\theta=90°$ does not enable one to choose between the signs of F_π. This is because the contribution of the π^0-meson pole for $\theta=90°$ is small in this energy range. On the other hand, analysis of the experimental data for the angle $\theta=150°$ gives the sign $g_{\pi NN}F_\pi<0$ [the probabilities $P_f(\chi^2)$ for the competing hypotheses are 1.3 and 0.7%]. This sign of F_π agrees with the sign found in Refs. 75, 76, 87, and 88 from the analysis of γp scattering by means of dispersion relations.

Thus, investigation of γp scattering in the region of low energies by means of the expression (69) enables one to determine the sign of the $\pi^0\to2\gamma$ decay amplitude in a model-independent manner and with a fairly reliable estimate of the terms $O(\nu^4)$ omitted in this expression.

Sum rules for coefficients of the generalized polarizability of the proton

Good agreement with the $\bar{\alpha}$ and $\bar{\beta}$ values (67) was obtained by Fedyanin.[65] For a certain new set of invariant amplitudes different from (9), Fedyanin constructed subtracted dispersion relations for fixed t, determining the subtraction functions in terms of the low-energy limit. These dispersion relations were saturated by the amplitudes of single-pion photoproduction in the energy range up to 1 GeV and were calculated for $\nu=55$ MeV; the results were $\bar{\alpha}=10.4\times10^{-43}$ cm^3 and $\bar{\beta}=0.7\times10^{-43}$ cm^3.

However, it should be borne in mind that the t dependence of the subtraction functions was not taken into account in the dispersion relations, so that the contribution of the annihilation channel was ignored.

In Ref. 111, Bernabeu *et al.* considered dispersion relations for the amplitude proportional to the amplitude difference R_1-R_2 for the angle $\theta=180°$ and obtained sum rules for $\bar{\alpha}-\bar{\beta}$. In these sum rules, the contribution of the annihilation channel, which was assumed to be small, was ignored. Calculations with allowance for (65) gave the following results: $\bar{\alpha}=4\times10^{-43}$ cm^3 and $\bar{\beta}=10\times10^{-43}$ cm^3. Thus, these calculations indicated $\bar{\beta}>\bar{\alpha}$, in disagreement with the experimental data.

A similar result is obtained if one writes down once-subtracted dispersion relations for angle 0° for the amplitudes R_1 and R_2 separately. This is because the main contribution to $\bar{R}_1$ comes from the integral of E_{0^+}, and that to $\bar{R}_2$ from the integral of M_{1^+}. The disagreement with experiment probably indicates the impossibility of constructing once-subtracted dispersion relations for the amplitudes R_1 and R_2 (and also R_1-R_2) at angle $\theta=0°$.

Akhmedov and Fil'kov[112] expressed the amplitude difference R_1-R_2 for $\theta=0°$ in terms of the amplitudes T_i in (9), for which they then wrote down the dispersion relations (33) and (35).

From the relations (14) one readily obtains

$$R_1(\nu, z=1)-R_2(\nu, z=1)=-\frac{\nu^2}{2W}(T_2+T_4)_{z=1}-\frac{\partial}{\partial z}[(T_1+T_3)+\nu(T_2+T_4)]_{z=1}, \tag{70}$$

where $z=\cos\theta$ and $W^2=s=m^2+2m\nu$.

For the amplitudes T_1 and T_3 we rewrite the dispersion relation (42) in the form

$$\mathrm{Re}\,T_i(\nu, t)=r_i\left(\frac{1}{m^2-s}+\frac{1}{m^2-u}\right)+T_i(m^2, 0)+t\phi_i(t, u=m^2)+\frac{\nu}{\pi}P\int_{\nu_0}^{\infty}d\nu' A_1^{(s)}(\nu', t)\times\left[\frac{1}{\nu'(\nu'-\nu)}-\frac{1}{(\nu'+t/2m)(\nu'+\nu+t/2m)}\right]. \tag{71}$$

The dispersion relation (35) for the amplitudes T_2 and T_4 can also be expressed in terms of the variable ν:

$$\mathrm{Re}\,T_j(\nu, t)=r_j\left(\frac{1}{m^2-s}-\frac{1}{m^2-u}\right)+\frac{4m\nu+t}{2\pi m}P\int_{\nu_0}^{\infty}\frac{A_j^{(s)}(\nu', t)\,d\nu'}{(\nu'-\nu)(\nu'+\nu+t/2m)}, \quad j=2, 4. \tag{72}$$

Substituting (71) and (72) into (70) and retaining only the terms with ν^2, we obtain

$$\bar{R}_1(\nu, z=1)-\bar{R}_2(\nu, z=1)=\nu^2\{[2(r_1+r_3)/m+(r_2+r_4)/2]/m^3-2\Lambda_+(0)\}, \tag{73}$$

where $\Lambda_+(0)=\phi_1(0)+\phi_3(0)$. Taking into account (61), we find the following sum rules for the difference $\bar{\alpha}-\bar{\beta}$ of the polarizabilities[110]:

$$\bar{\alpha}-\bar{\beta}=e^2[(1+\lambda_p)^2/4-4,5]/4\pi m^3-\Lambda_+(0)/2\pi. \tag{74}$$

In this expression, $\Lambda_+(0)$ has in accordance with (45) the form

$$\Lambda_+(0)=\frac{1}{\pi}\int\limits_{4\mu^2}^{\infty}\frac{dt'}{t'^2}[A_1^{(t)}(t',\,u=m^2)+A_3^{(t)}(t',\,u=m^2)]$$

$$-\frac{1}{\pi}\int\limits_{(m+\mu)^2}^{\infty}\frac{A_1^{(s)}(s',\,u=m^2)+A_3^{(s)}(s',\,u=m^2)}{(s'-m^2)^2}ds'.$$

We take into account the contribution of the two-particle $\pi\pi$ interaction to the first integral by means of the diagrams shown in Fig. 10. We shall saturate the integrals of $A_1^{(s)}$ and $A_3^{(s)}$ by the single-pion photoproduction amplitudes, using the multipole analyses of Ref. 80 (up to 250 MeV) and Ref. 114 (from 250 to 1200 MeV). Since the second integral contains the imaginary parts of the amplitudes in the s channel for fixed $u=m^2$, which corresponds to an unphysical value of $\cos\theta$, the partial-wave series for these amplitudes may diverge. Therefore, we sum the series in $\cos\theta$ in the amplitudes $A_1^{(s)}(s',\,u=m^2)$ and $A_3^{(s)}(s',\,u=m^2)$ by means of the [1, 1] and [1, 2] Padé approximants. We obtain

$$\bar{\alpha}-\bar{\beta}=15.3\times10^{-43}\ \text{cm}^3. \tag{75}$$

The main contribution to $\Lambda_+(0)$, and therefore to $\bar{\alpha}-\bar{\beta}$, is the annihilation channel's. The contribution of the second integral is only about 5%. Therefore, the sum rules (74) can serve as a good tool for selecting between different models with allowance for the contribution of the t channel to γp scattering. It should be noted that if no summation is performed over $\cos\theta$ in the amplitudes $A_1^{(s)}(s',m^2)$ and $A_3^{(s)}(s',m^2)$ by means of Padé approximants, the contribution of the second integral is about 10%.

In order to take into account in $\Lambda_+(0)$ the contribution from the t-channel states not covered by the diagrams in Fig. 10, we use the bootstrap model (36), relating the integrals of the amplitudes in the t channel to the integrals of the amplitudes in the s channel, as was done in analysis of the dispersion relations for the γp scattering amplitudes:

$$\Lambda_+(0)=\frac{1}{\pi}\int\limits_{4\mu^2}^{\infty}\frac{[A_1^{(t)}(t',\,u=m^2)+A_3^{(t)}(t',\,u=m^2)]^B}{t'^2}dt'$$

$$-\frac{1}{\pi}\int\limits_{(m+\mu)^2}^{\infty}\frac{[A_1^{(s)}(s',\,u=m^2)+A_3^{(s)}(s',\,u=m^2)]^B}{(s'-m^2)^2}ds' \tag{76}$$

$$+\frac{1}{\pi}\int\limits_{(m+\mu)^2}^{\infty}\frac{ds'}{s'-m^2}\left\{2\,\frac{\partial}{\partial t}[\bar{A}_1^{(s)}(s',\,t)+\bar{A}_3^{(s)}(s',\,t)]_{t=0}\right.$$

$$\left.-\frac{\bar{A}_1^{(s)}(s',\,t=0)+\bar{A}_3^{(s)}(s',\,t=0)}{s'-m^2}\right\},$$

where the first two integrals take into account only the contribution of the diagrams in Fig. 10, and the bar above $A_1^{(s)}$ and $A_3^{(s)}$ means that the contribution from these diagrams is omitted in these amplitudes. Using as before the analyses of Refs. 80 and 114 in (76), we obtain

$$\bar{\alpha}-\bar{\beta}=12.3\times10^{-43}\ \text{cm}^3. \tag{77}$$

If we sum the series in $\cos\theta$ by means of Padé approximants in the amplitudes $A_1^{(s)}(s',t)$ and $A_3^{(s)}(s',t)$ and then calculate the derivative with respect to t in (76), we obtain

$$\bar{\alpha}-\bar{\beta}=10.4\times10^{-43}\ \text{cm}^3. \tag{78}$$

The integral of $\bar{A}_1^{(s)}(s',0)+\bar{A}_3^{(s)}(s',0)$ has remained practically the same, and all the changes have been due to allowance for the integral of the derivative with respect to t. This indicates that the partial-wave series in the expression $\partial[A_1^{(s)}(s',t)+A_3^{(s)}(s',t)]/dt$ does not converge sufficiently rapidly, and in this case one must use methods of approximate summation. This must be borne in mind when one is investigating γp scattering by means of dispersion relations.

As can be seen from (75), (77), and (78) with allowance for (65), the sum rules discussed here[112] give $\alpha>\beta$ for all models, in agreement with the experiments. It would be interesting to take into account the contribution of the σ meson to $\Lambda_+(0)$. This contribution must increase the value of $\bar{\alpha}-\bar{\beta}$ compared with (75).

CONCLUSIONS

Thus, our investigation of the elastic scattering of γ's on protons at low and medium energies enables us to draw the following conclusions:

1. From a comparison of the experimental data with the prediction of dispersion relations for fixed t the sign of the $\pi^0\to2\gamma$ decay amplitude was determined for the first time ($g_{\pi NN}F_\pi<0$); it is an important parameter in the construction of various field-theory models. Later, this sign was confirmed in π^0-meson photoproduction experiments.

2. Comparison of theory and experiment at energies below 150 MeV and from 230 to 280 MeV indicates that one must take into account in the annihilation channel not only the fourth-order diagrams (see Fig. 10) but also other states as well (for example, by means of the bootstrap model).

3. In the range of energies 180—220 MeV and in the region of the P_{33} resonance (for $\theta=90°$) there is a strong discrepancy between the experiments and the predictions of the dispersion relations. In the region of the P_{33} resonance a discrepancy is obtained even for the lower limit of the theoretical predictions for the differential cross section of scattering at angle $\theta=90°$. All this indicates that further theoretical investigations must be made, as well as new experimental measurements of γp scattering in these energy regions.

4. Investigation of γp scattering at low energies led to the discovery of the polarizability of the proton and made it possible to determine the coefficients of the generalized electric and magnetic polarizability of the proton. At the present time, the γp scattering process at low energies is the only source of information about these parameters.

5. With a view to obtaining the polarizability coefficients of the proton from γp scattering experiments, an expression was obtained from the general requirements of quantum field theory for the differential cross section of γp scattering as a series in the γ energy, including ν^3 terms. We have shown that in this expression for the differential cross section it is necessary to take into account the π^0-meson pole. The difference of the coefficients of the electric and the magnetic polarizabil-

ity is particularly sensitive to this. In order to determine more accurately the coefficients, it is necessary to estimate more accurately the terms omitted in the expression for the cross section and make new measurements of the energy dependence of γp scattering (for example, for angles $\theta = 90$ and $150°$) in the energy range 20–100 MeV with a better energy resolution.

6. Evaluation of the experimental γp-scattering data in the energy range 80–110 MeV by means of the expression (69) for the differential cross section yielded the sign of the $\pi^0 \to 2\gamma$ decay amplitude, which agrees with the sign obtained previously by comparing the γp-scattering data at low and medium energies with the prediction of the dispersion relations.

7. Comparison of the experimental data for the difference of the electric and magnetic polarizabilities of the proton with the results of calculations made with sum rules enables one to analyze the various models used to take into account the annihilation channel in the dispersion relations for the γp-scattering amplitudes.

8. Analysis of the Gerasimov–Drell–Hearn sum rules yields additional information about the Regge trajectories with negative τP.

9. Further analysis of the sum rules for the $\pi^0 \to 2\gamma$ decay amplitude will make it possible to establish whether there is a fixed pole with the quantum numbers of the π^0 meson.

[1]A. I. Akhiezer and V. G. Berestetskiĭ, Kvantovaya Élektrodinamika, Nauka, Moscow (1969) [translation of earlier edition: Quantum Electrodynamics, New York, (1965)].
[2]R. Yu. Volkovyskiĭ, Yad. Fiz. **2**, 878 (1965) [Sov. J. Nucl. Phys. **2**, 626 (1966)].
[3]L. G. Hyman *et al.*, Phys. Rev. Lett. **3**, 93 (1959).
[4]V. N. Baier *et al.*, Preprint, Nucl. Phys. Inst., Siberian Division, Acad. Sci. USSR, 58-73/in Russian/(1973).
[5]R. I. Dzhikibaev *et al.*, Pis'ma Zh. Éksp. Teor. Fiz. **19**, 73 (1974) [JETP Lett. **19**, 47 (1974)].
[6]R. C. Miller, Phys. Rev. **95**, 796 (1954).
[7]R. F. Stiening, E. Loh, and M. Deutsch, Phys. Rev. Lett. **10**, 536 (1963).
[8]L. W. Alvarez, F. S. Crawford, and M. L. Stevenson, Phys. Rev. **112**, 1267 (1958).
[9]V. I. Gol'danskiĭ *et al.*, Zh. Éksp. Teor. Fiz. **38**, 1695 (1960) [Sov. Phys. JETP **11**, 1223 (1960)].
[10]C. L. Oxley and V. L. Telegdi, Phys. Rev. **100**, 435 (1955).
[11]C. L. Oxley and V. L. Telegdi, Nuovo Cimento, Suppl. 2, **4**, 953 (1956).
[12]C. L. Oxley, Phys. Rev. **110**, 733 (1958).
[13]B. B. Govorkov *et al.*, Dokl. Akad. Nauk SSSR **110**, 988 (1956).
[14]L. Higgins, thesis, California Univ., UCRL-3688 (1957).
[15]P. S. Baranov *et al.*, Pis'ma Zh. Éksp. Teor. Fiz. **19**, 777 (1974) [JETP Lett. **19**, 398 (1974)].
[16]P. S. Baranov *et al.*, Phys. Lett. B **52**, 122 (1974).
[17]P. S. Baranov *et al.*, Preprint FIAN, No. 93/in Russian/, P. N. Lebedev Physics Institute (1974).
[18]P. S. Baranov *et al.*, Zh. Éksp. Teor. Fiz. **41**, 1713 (1961) [Sov. Phys. JETP **14**, 1219 (1962)].
[19]P. S. Baranov *et al.*, Zh. Éksp. Teor. Fiz. **50**, 364 (1966) [Sov. Phys. JETP **23**, 242 (1966)].
[20]P. S. Baranov *et al.*, Yad. Fiz. **3**, 1083 (1966) [Sov. J. Nucl. Phys. **3**, 791 (1966)]
[21]G. Bernardini *et al.*, Nuovo Cimento **18**, 1203 (1960).
[22]E. Gray, Ph. D. thesis, Univ. of Illinois, USA (1966); E. R. Gray and A. O. Hanson, Abstracts. Int. Conf. on Low and Intermediate Energy Electromagnetic Interactions, Dubna (1967); Phys. Rev. **160**, 1212 (1967).
[23]L. Hyman, MIT. Ph. D. thesis (1959).
[24]S. Kate *et al.*, Ann. Report INSU Tokyo, 77 (1966).
[25]H. Genzel and W. Pfeil, Photoproduction Data Below 1.5 GeV, Bonn Univ. PI BI-168 (1972).
[26]H. Genzel *et al.*, Lett. Nuovo Cimento **4**, 695 (1972).
[27]J. W. Dewire *et al.*, Phys. Rev. **124**, 909 (1961).
[28]M. Jung, Ph. D. thesis, Phys. Inst. der Univ. Bonn 1-066, (1967); XV Int. Conf. on High Energy Phys., Kiev (1970).
[29]Y. Nagashima, Ph. D. thesis, INSU Tokyo, 81, TH-47 (1964).
[30]D. R. Rust *et al.*, Phys. Rev. Lett. **15**, 938 (1965).
[31]M. Deutsch *et al.*, Phys. Progr. Report MIT, N 358 (1967), p. 29.
[32]P. S. Baranov *et al.*, Yad. Fiz. **21**, 6 (1975) [Sov. J. Nucl. Phys. **21**, 355 (1975)].
[33]G. E. Pugh *et al.*, Phys. Rev. **105**, 982 (1957).
[34]D. Frisch, private communication (1967).
[35]J. I. Powell, Phys. Rev. **75**, 32 (1949).
[36]G. Buschhorn *et al.*, Phys. Lett. B **33**, 241 (1970).
[37]D. F. Jacob and M. Deutsch, XV Int. Conf. on High Energy Phys., Kiev (1970); Bull. Amer. Phys. Soc. **15**, 608 (1970).
[38]M. Deutsch *et al.*, MIT Progress Report, May (1963), p. 82.
[39]E. Loh *et al.*, MIT Progress Report, November (1963), p. 82.
[40]R. L. Anderson *et al.*, Phys. Rev. Lett. **25**, 1218 (1970).
[41]A. M. Boyarski *et al*, Phys. Rev. Lett. **26**, 1600 (1971).
[42]G. Barbiellini, G. Capon, and G. Murtas, Proc. of Int. Symp. on Electron and Photon Interactions, Hamburg, II, (1965), p. 343.
[43]R. E. Prange, Phys. Rev. **110**, 240 (1958),
[44]L. I. Lapidus and Chou Kuang-Chau, Zh. Éksp. Teor. Fiz. **37**, 1714 (1959) [Sov. Phys. JETP **10**, 1213 (1960)].
[45]A. C. Hearn and E. Leader, Phys. Rev. **126**, 789 (1962).
[46]V. I. Ritus, Zh. Éksp. Teor. Fiz. **33**, 1264 (1957) [Sov. Phys. JETP **6**, 972 (1958)]; L. I. Lapidus, Zh. Éksp. Teor. Fiz. **34**, 922 (1958) [Sov. Phys. JETP **7**, 638 (1958)].
[47]V. I. Ritus, Dissertation/in Russian/, P. N. Lebedev Physics Institute (1959).
[48]M. Gell-Mann, M. L. Goldberger, and W. E. Thirring, Phys. Rev. **95**, 1612 (1954).
[49]H. A. Kramers, Atti Congr. Internat. Fisici, Como, **2**, 545 (1927); R. Kronig, Physica **12**, 543 (1946).
[50]N. N. Bogolyubov and D. V. Shirkov, Dokl. Akad. Nauk SSSR **113**, 529 (1957).
[51]A. A. Logunov and P. S. Isaev, Nuovo Cimento **10**, 917 (1958).
[52]N. N. Bogolyubov, Int. Conf. on Theoret. Phys., Seattle (1956); N. N. Bogolyubov, B. V. Medvedev, and M. K. Polivanov, Voprosy Teorii Dispersionnykh Sootnosheniĭ (Aspects of the Theory of Dispersion Relations), Fizmatgiz, Moscow (1958).
[53]R. Oehme and J. G. Taylor, Phys. Rev. **113**, 371 (1959).
[54]M. Cini and R. Stroffolini, Nucl. Phys. **5**, 684 (1958).
[55]R. H. Capps, Phys. Rev. **106**, 1031 (1957); **108**, 1032 (1957).
[56]J. Mathews, Ph. D. thesis, California Inst. of Technol. (1957).
[57]T. Akiba and I. Sato, Progr. Theor. Phys. **19**, 93 (1958).
[58]L. I. Lapidus and Chou Kuang-Chau, Zh. Éksp. Teor. Fiz. **41**, 1546 (1961) [Sov. Phys. JETP **14**, 1102 (1962)].
[59]M. Jacob and J. Mathews, Phys. Rev. **117**, 854 (1960).
[60]L. I. Lapidus and Chou Kuang-Chau, Zh. Éksp. Teor. Fiz. **41**, 294 (1961) [Sov. Phys. JETP **14**, 210 (1962)].
[61]M. L. Goldberger and S. B. Treiman, Nuovo Cimento **9**, 451 (1958).
[62]A. P. Contogouris, Phys. Rev. **124**, 912 (1961).
[63]A. P. Contogouris and A. Vergenelakis, Phys. Lett. **6**, 103 (1963).
[64]V. F. Müller, Z. Phys. (Germany) **170**, 114 (1962).
[65]V. K. Fedyanin, Dokl. Akad. Nauk SSSR **140**, 347 (1961); Zh. Éksp. Teor. Fiz. **44**, 633 (1963) [Sov. Phys. JETP **17**,

429 (1963)].
[66]A. P. Contogouris, Nuovo Cimento **25**, 104 (1962).
[67]D. Holliday, Ann. Phys. (N.Y.) **24**, 289, 319 (1963).
[68]S. Mandelstam, Phys. Rev. **112**, 1344 (1958).
[69]R. Köberle, Phys. Rev. **166**, 1558 (1968).
[70]J. Hamilton *et al.*, Phys. Rev. **128**, 1881 (1962).
[71]L. V. Fil'kov and N. F. Nelipa, Int. Conf. on High Energy Phys., CERN (1952), p. 225; Nucl. Phys. **59**, 225 (1964).
[72]L. V. Fil'kov, Yad. Fiz. **2**, 352 (1965) [Sov. J. Nucl. Phys. **2**, 251 (1966)].
[73]L. V. Fil'kov, Yad. Fiz. **3**, 336 (1966) [Sov. J. Nucl. Phys. **3**, 242 (1966)].
[74]L. V. Fil'kov, Tr. Fiz. Inst. Akad. Nauk SSSR **41**, 3 (1967).
[75]P. S. Baranov, L. V. Fil'kov, and G. A. Sokol, Fortschr. der Phys. **16**, 595 (1968).
[76]P. S. Baranov, A. V. Dembovskiĭ, and L. V. Fil'kov, Kratkie Soobshcheniya po Fizike, FIAN, No. 3, 16 (1970).
[77]V. Barger and D. Cline, Phys. Rev. Lett. **16**, 913 (1966).
[78]W. Pfeil, H. Rollnik, and S. Stankowski, Nucl. Phys. B **73**, 166 (1974).
[79]P. Noelle, W. Pfeil, and D. Schwela, Nucl. Phys. B **26**, 461 (1971).
[80]W. Pfeil and D. Schwela, Nucl. Phys. B **45**, 379 (1972).
[81]F. A. Berends and D. L. Weaver, Nucl. Phys. B **30**, 575 (1971).
[82]R. L. Walker, Phys. Rev. **182**, 1729 (1969).
[83]L. V. Fil'kov, Yad. Fiz. **12**, 380 (1970) [Sov. J. Nucl. Phys. **12**, 209 (1971)].
[84]L. V. Fil'kov and A. G. Grigoryants, Nucl. Phys. B **36**, 141 (1972).
[85]C. Bemporad *et al.*, Int. Conf. on Low and Intermediate Energy Electromagnetic Interactions, Dubna (1967).
[86]A. Browman *et al.*, Phys. Rev. Lett. **32**, 1067 (1974).
[87]P. S. Baranov *et al.*, Yad. Fiz. **5**, 1221 (1967) [Sov. J. Nucl. Phys. **5**, 873 (1967)].
[88]P. S. Baranov *et al.*, Yad. Fiz. **7**, 100 (1968) [Sov. J. Nucl. Phys. **7**, 73 (1968)].
[89]M. V. Terent'ev, Usp. Fiz. Nauk **112**, 37 (1974) [Sov. Phys. Uspekhi **17**, 20 (1974)].
[90]S. Okubo, Phys. Rev. **179**, 1629 (1969).
[91]F. J. Gilman, Phys. Rev. **184**, 1964 (1969).
[92]N. P. Zotov, Yu. A. Rakov, and V. A. Tsarev, Kratkie Soobshcheniya po Fizike, FIAN, No. 8, 37 (1970).
[93]W. A. Bardeen and Wu-Ki Tung, Phys. Rev. **173**, 1423 (1968).
[94]Yu. M. Aleksandrov *et al.*, Proc. Symp. on Electron and Photon Interactions at High Energies, Bonn (1973), p. 518.
[95]S. B. Gerasimov, Yad. Fiz. **2**, 598 (1965) [Sov. J. Nucl. Phys. **2**, 430 (1966)].
[96]S. D. Drell and A. C. Hearn, Phys. Rev. Lett. **16**, 908 (1966).
[97]V. Ya. Faĭnberg and L. V. Fil'kov, Pis'ma Zh. Éksp. Teor. Fiz. **5**, 64 (1967) [JETP Lett. **5**, 51 (1967)]; L. V. Fil'kov, Yad. Fiz. **12**, 380 (1970); [Sov. J. Nucl. Phys. **12**, 209 (1971)].
[98]H. Pagels, Phys. Rev. **158**, 1566 (1968).
[99]H. D. I. Abarbanel and M. L. Goldberger, Phys. Rev. **165**, 1594 (1968); S. R. Choudhury and R. Rajaraman, Phys. Rev. **169**, 1218 (1968).
[100]F. E. Low, Phys. Rev. **96**, 1428 (1954).
[101]M. Gell-Mann and M. L. Goldberger, Phys. Rev. **96**, 1433 (1954).
[102]A. Klein, Phys. Rev. **99**, 998 (1955).
[103]A. M. Baldin, Nucl. Phys. **18**, 310 (1960).
[104]V. A. Petrun'kin, Zh. Éksp. Teor. Fiz. **40**, 1148 (1961) [Sov. Phys. JETP **13**, 808 (1961)]; Tr. Fiz. Inst., Akad. Nauk SSSR **41**, 165 (1967).
[105]V. S. Barashenkov, H. J. Kaiser, and A. A. Ogreba, Phys. Lett. **2**, 33 (1962).
[106]V. S. Barashenkov and H. J. Kaiser, Fortschr. der Phys. **10**, 33 (1962); V. S. Barashenkov *et al.*, Nucl. Phys. **50**, 684 (1964).
[107]L. I. Lapidus, Zh. Éksp. Teor. Fiz. **43**, 1358 (1962) [Sov. Phys. JETP **16**, 964 (1963)].
[108]A. S. Belousov *et al.*, Dokl. Akad. Nauk SSSR **215**, 76 (1974).
[109]P. Joos, Preprint DESY-HERA 70-1 (1970).
[110]P. S. Baranov, L. V. Fil'kov, and L. N. Shtarkov, Pis'ma Zh. Éksp. Teor. Fiz. **20**, 762 (1974) [JETP Lett. **20**, 353 (1974)].
[111]J. Bernabeu, T. E. O. Ericson, and C. FerroFontan, Phys. Lett. B **49**, 381 (1974).
[112]D. M. Akhedov and L. V. Fil'kov, Kratkie Soobshcheniya po Fizike, FIAN, No. 1, 13 (1975).
[113]N. Barash-Schmidt and A. Barbaro-Galtieri, Phys. Lett. B **50**, 1 (1974).
[114]R. G. Moorhouse, H. Oberlack, and A. H. Rosenfeld, Phys. Rev. D **9**, 1 (1974).
Translated by Julian B. Barbour.